PCCP

ROYAL SOCIETY OF CHEMISTRY

PAPER

View Article Online
View Journal | View Issue

Cite this: *Phys. Chem. Chem. Phys.*, 2021, **23**, 19054

Exploring vibronic coupling in the benzene radical cation and anion with different levels of the *GW* approximation†

Zi Cheng Wong * and Liviu Ungur

Received 21st June 2021,
Accepted 6th August 2021

DOI: 10.1039/d1cp02795f

rsc.li/pccp

The linear vibronic coupling constants of the benzene radical cation and anion have been obtained with different levels of the *GW* approximation, including G_0W_0, eigenvalue self-consistent *GW*, and quasiparticle self-consistent *GW*, as well as DFT with the following exchange–correlation functionals: BLYP, B3LYP, CAM-B3LYP, tuned CAM-B3LYP, and an IP-tuned CAM-B3LYP functional. The vibronic coupling constants were calculated numerically using the gradients of the eigenvalues of the degenerate HOMOs and LUMOs of the neutral benzene molecule for DFT, while the numerical gradients of the quasiparticle energies were used in the case of *GW*. The results were evaluated against those of high level wave function methods in the literature, and the approximate self-consistent *GW* methods and G_0W_0 with long-range corrected functionals were found to yield the best results on the whole.

1 Introduction

The ability to interpret and predict chemistry-related phenomena ranging from organic reactivity to molecular spectroscopy is one of the ultimate goals of computational quantum chemistry. However, this requires an exact solution to the Schrödinger equation of the system of interest, which is impossible in almost all situations. Because of this, simplifying approximations are necessary to reduce the complexity of the problem and render it solvable.

A common starting point is to treat the nuclear and electronic motion separately by applying the adiabatic approximation.[1] The electronic wave functions and their corresponding energies are first obtained by solving the electronic Schrödinger equation, which is dependent on the nuclear coordinates parametrically. The adiabatic potential energy surface (PES) associated with a particular electronic eigenstate is then the variation of the corresponding electronic energy with respect to the nuclear coordinates.[1]

The potential energy for nuclear motion is given by the adiabatic PES, and can be applied to examine and interpret various chemical processes. For example, the PES can be used to predict and simulate molecular rotational and vibrational spectra, and *vice versa*.[2,3] Other than this, knowledge of the PES is also essential towards gaining an understanding of how biological macromolecules fold to form complex three-dimensional structures.[4,5]

However, the adiabatic approximation is sufficient only when the coupling between the electronic and nuclear motion is negligible. It is inadequate for treating systems with significant non-adiabatic effects; *e.g.* degenerate electronic states or conical intersections. Vibronic coupling, which is the coupling between the electronic and vibrational motion of a molecule, has to be taken into consideration to model such systems properly.[6,7] For example, vibronic coupling can be used to rationalise the symmetry breaking distortion of electronically degenerate systems in the Jahn–Teller (JT) theorem.[8]

As its name would suggest, the prerequisites of studying vibronic coupling are an accurate treatment for both the vibrational and electronic motion. As such, a quantitatively accurate description of the molecular electronic and vibrational structure is crucial for the calculation of vibronic coupling constants. Highly correlated wave function methods, such as coupled-cluster singles and doubles with perturbative triples (CCSD(T))[9,10] or complete-active-space with second-order perturbation theory (CASPT2),[11,12] have been shown to fulfil the above criteria for accuracy, but the high computational cost of these methods precludes their usage for larger molecules.[13–16]

A popular option in computational chemistry is Kohn–Sham density functional theory (DFT).[17–19] The main challenge in the use of Kohn–Sham DFT lies in the choice of an appropriate exchange–correlation functional. Depending on the exchange–correlation functional used, the quality of the DFT results can vary from being qualitatively wrong to yielding values

Department of Chemistry, National University of Singapore, Block S8 Level 3, 3 Science Drive 3, 117543, Singapore. E-mail: chmwzc@nus.edu.sg

† Electronic supplementary information (ESI) available: Details of the IP-tuning procedure, vibrational frequencies, the effect of the basis set and normal mode coordinates, second order vibronic coupling, and the full set of numerical results. See DOI: 10.1039/d1cp02795f

comparable to the CCSD(T) level of theory.[19–24] As a result, the development and benchmarking of exchange–correlation functionals in DFT remain a topic of great interest, even today.[21,22,25,26]

Alternatively, a possible method that has been shown to improve upon the shortcomings of DFT is the *GW* approximation, which is based on Green's function in many-body perturbation theory.[27,28] The one-particle Green's function for an interacting system is connected to the Green's function for a non-interacting system by a Dyson equation, which includes a self-energy term containing all electron correlation effects.[29] Thus, the main challenge in Green's function-based approaches lies in finding a suitable approximation for the self-energy term.

Hedin approached this problem by first expanding the self-energy as a series in terms of the Green's function G and a screened Coulomb interaction W.[30] This is followed by the neglect of vertex corrections, which gives an expression for the self-energy to be iGW, and hence the name of the *GW* approximation. Notwithstanding these simplifications, Hedin's equations with the *GW* approximation still has to be solved self-consistently, which remains a computationally demanding task.

As such, the G_0W_0 method is frequently used instead. In the 'one-shot' G_0W_0 approach, the *GW* quasiparticle energies are computed perturbatively with respect to the one-electron eigenvalues obtained from a mean-field Hartree–Fock (HF) or DFT calculation.[28,31,32] G_0W_0 has been shown to improve upon some problems with DFT; the ionisation potentials (IPs) and band gaps calculated with G_0W_0 are often improved compared to the corresponding DFT starting points.[31,33–36] However, as G_0W_0 only acts as a single perturbative correction, it remains strongly dependent on the initial mean-field calculation.[32,33,37]

To reduce this starting point dependence, a few simplified self-consistent *GW* methods have been proposed to extend and improve upon the G_0W_0 approach. In eigenvalue self-consistent *GW* (ev*GW*), the eigenvalues of the quasiparticle equation are calculated self-consistently by re-entering the quasiparticle energies into the computation of G, W, and the self-energy.[36,38,39] A simplified form of ev*GW* is to update only G and not W (evGW_0), such that the screened Coulomb interaction W_0 is only calculated once using the eigenvalues from the mean-field calculation.[39,40] In both ev*GW* and evGW_0, the quasiparticle wave function is kept unchanged throughout, while the quasiparticle energies are computed iteratively. In contrast, the quasiparticle wave function and energies are both obtained self-consistently in the quasiparticle self-consistent *GW* (qs*GW*) method, which uses an energy-independent and Hermitian approximation to the *GW* self-energy operator to simplify the quasiparticle equation.[38,41,42]

The effect of going beyond G_0W_0 with these approximate self-consistent *GW* methods has been found to be largely positive, with a reduced dependence on the initial mean-field calculation in conjunction with an improvement in the computed IPs.[34,38,43–46] Naturally, the price of these improvements is an increased computational cost, compared to that of G_0W_0.

Although there is a growing interest in *GW* in the context of vibronic coupling,[47–55] these studies are largely limited to G_0W_0, and the results of going up the hierarchy of *GW* methods remains to be studied. In an earlier study, we derived the vibronic coupling constants of the cyclopentadienyl radical using the gradients of the G_0W_0 quasiparticle energies.[47] Our results were mostly in agreement with those of the high level wave function methods, but the starting point dependence of the computed vibronic coupling constants was still noticeable. Hence, to mitigate this starting point dependence, the present study aims to investigate the ev*GW*, evGW_0, and qs*GW* methods towards computing the vibronic coupling constants of the benzene radical cation and anion.

The benzene radical cation has been the subject of numerous experimental and computational studies in the context of the JT effect.[56–77] Köppel and co-workers have carried out a series of studies examining the vibronic interactions in the benzene radical cation, in which the vibronic coupling constants are first obtained using *ab initio* calculations, before being used in quantum dynamics simulations to characterise the internal conversion processes in the benzene cation.[56–61] Johnson and co-workers interpreted the photoinduced Rydberg ionization and mass-analysed threshold ionization spectra of benzene using the vibronic coupling constants calculated with DFT.[62–64] Applegate and Miller analysed the zero kinetic energy spectra of benzene in a similar manner using the complete active space self-consistent field (CASSCF) calculations.[65] More recently, Vidal *et al.* simulated the X-ray absorption spectra of neutral benzene and its cation using equation-of-motion coupled-cluster methods.[66] The difference between the two was attributed to the splitting of the $1s_C \rightarrow \pi^*$ transition in the JT-distorted benzene cation.[67]

There are far fewer studies on the JT effect in the benzene radical anion in comparison,[78–82] with some investigating both the benzene cation and anion within a single work.[83–86] Tokunaga *et al.* derived the vibronic coupling constants as the integral over the electronic operator of a vibronic Hamiltonian, which was then computed using generalised HF and CASSCF calculations.[83] Kato and co-workers used the same approach, except with DFT.[84,85] Perebeinos *et al.* used a model Hückel-type electronic Hamiltonian to investigate the electron–phonon coupling in the bond stretching and bending vibrational modes.[86]

Hence, the performance of *GW* towards the calculation of vibronic coupling constants can be examined using these studies. The rest of this work is structured as follows. The theory behind the calculation of the vibronic coupling constants of the benzene radical cation and anion and an overview of the various *GW* methods used in this work are given in Section 2. Computational details are given in Section 3, followed by the results and discussion in Section 4 and concluding remarks in Section 5.

2 Theory

2.1 Vibronic coupling

We follow the protocol by Tokunaga *et al.* in this work.[83,87] The Hamiltonian for a molecular system, H_{mol}, can be written as

$$H_{\mathrm{mol}}(\boldsymbol{r},\boldsymbol{R}) = T_{\mathrm{n}}(\boldsymbol{R}) + T_{\mathrm{e}}(\boldsymbol{r}) + U_{\mathrm{nn}}(\boldsymbol{R}) + U_{\mathrm{ne}}(\boldsymbol{r},\boldsymbol{R}) + U_{\mathrm{ee}}(\boldsymbol{r}) \quad (1)$$

where T_{n} and T_{e} represent the kinetic energy operators for the nuclei and electrons, respectively, while U_{nn}, U_{ne} and U_{ee} are the nuclear–nuclear, nuclear–electron, and electron–electron electrostatic interactions. The nuclear and electronic coordinates of the molecule are given by $\boldsymbol{R}$ and $\boldsymbol{r}$, respectively. The electronic Hamiltonian for the molecule, H_{e}, is written as

$$H_{\mathrm{e}}(\boldsymbol{r},\boldsymbol{R}) = T_{\mathrm{e}}(\boldsymbol{r}) + U_{\mathrm{nn}}(\boldsymbol{R}) + U_{\mathrm{ne}}(\boldsymbol{r},\boldsymbol{R}) + U_{\mathrm{ee}}(\boldsymbol{r}). \quad (2)$$

The solution to the electronic Hamiltonian within the adiabatic approximation is then the electronic wave function, $\Psi_{\mathrm{k}}(\boldsymbol{r};\boldsymbol{R})$:

$$\hat{H}_{\mathrm{e}}\Psi_{\mathrm{k}}(\boldsymbol{r};\boldsymbol{R}) = E_{\mathrm{k}}(\boldsymbol{R})\Psi_{\mathrm{k}}(\boldsymbol{r};\boldsymbol{R}) \quad (3)$$

where E_{k} represents the adiabatic PES corresponding to the electronic state k. Within the crude adiabatic approximation,[88] the electronic wave function $\Psi_{\mathrm{k}}(\boldsymbol{r};\boldsymbol{R_0})$ at a set of reference nuclear coordinates, $\boldsymbol{R}_0$, is used as the basis of the electronic operators in the molecular Hamiltonian:

$$H_{\mathrm{e}}(\boldsymbol{r};\boldsymbol{R}) = H_{\mathrm{e}}(\boldsymbol{r};\boldsymbol{R}_0) + \Delta U(\boldsymbol{r};\boldsymbol{R}) \quad (4)$$

such that the change in energy with respect to a distortion from $\boldsymbol{R}_0$ is accounted for by $\Delta U(\boldsymbol{r};\boldsymbol{R})$, the change in the U_{ne} and U_{nn} potential terms:

$$\Delta U(\boldsymbol{r};\boldsymbol{R}) = (U_{\mathrm{ne}}(\boldsymbol{r};\boldsymbol{R}) - U_{\mathrm{ne}}(\boldsymbol{r};\boldsymbol{R}_0)) + (U_{\mathrm{nn}}(\boldsymbol{R}) - U_{\mathrm{nn}}(\boldsymbol{R}_0)). \quad (5)$$

The vibronic Hamiltonian H_{vib} can be obtained by expanding the nuclear geometry about $\boldsymbol{R}_0$ in terms of mass-weighted normal coordinates Q_i:

$$\begin{aligned} H_{\mathrm{vib}} &= \sum_i -\frac{\hbar^2}{2}\left(\frac{\partial^2}{\partial Q_i^2}\right) + H_{\mathrm{e}}(\boldsymbol{r};\boldsymbol{R}_0) \\ &+ \sum_i \left(\frac{\partial U}{\partial Q_i}\right)_{R_0} Q_i \\ &+ \frac{1}{2!}\sum_i\sum_j \left(\frac{\partial^2 U}{\partial Q_i Q_j}\right)_{R_0} Q_i Q_j + \cdots \end{aligned} \quad (6)$$

where the indices $i, j = 1, 2, 3, \ldots, 3N - 6$ refer to the normal modes of the molecule ($3N - 5$ in the case of a linear molecule), and U is the sum of U_{ne} and U_{nn}. The third term onwards in eqn (6) corresponds to ΔU in eqn (4), and the nth order vibronic coupling constant $V^{(n)}_{i_1 i_2 \ldots i_n}$ is defined to be:

$$V^{(n)}_{i_1 i_2 \ldots i_n} = \left(\frac{\partial^n U}{\partial Q_{i_1}\partial Q_{i_2}\ldots\partial Q_{i_n}}\right)_{\boldsymbol{R}_0}. \quad (7)$$

Defining a zeroth-order Hamiltonian

$$H^{(0)} = \sum_i -\frac{\hbar^2}{2}\left(\frac{\partial^2}{\partial Q_i^2}\right) + H_{\mathrm{e}}(\boldsymbol{r};\boldsymbol{R}_0), \quad (8)$$

the vibronic Hamiltonian, H_{vib}., can be written as the sum of $H^{(0)}$ and the vibronic coupling terms:

$$H_{\mathrm{vib.}} = H^{(0)} + \sum_i V_i^{(1)} Q_i + \frac{1}{2!}\sum_{i_1}\sum_{i_2} V^{(2)}_{i_1 i_2} Q_{i_1} Q_{i_2} + \cdots. \quad (9)$$

As the present study is restricted to a linear vibronic coupling model, the intermode and higher order vibronic coupling terms can be removed from eqn (9), which gives

$$H_{\mathrm{vib.}} = H^{(0)} + \sum_i V_i^{(1)} Q_i + \frac{1}{2}\sum_i \omega_i^2 Q_i^2 \quad (10)$$

where ω_i is the vibrational frequency of the normal mode i.

The linear vibronic coupling term in eqn (10) can be written as the sum of one-electron operators and a nuclear–nuclear repulsion term, corresponding to the change in U_{ne} and U_{nn} with respect to the molecular geometry (eqn (5)). The linear vibronic coupling operator is then

$$\begin{aligned} \hat{V}_i^{(1)} &= -\sum_a\sum_\alpha \left[\frac{\partial}{\partial Q_i}\left(\frac{Z_\alpha e^2}{|\boldsymbol{r}_a - \boldsymbol{R}_\alpha|}\right)\right]_{\boldsymbol{R}_0} + \frac{\partial U_{\mathrm{nn}}}{\partial Q_i} \\ &= \sum_a \hat{v}_i^{(1)} + \frac{\partial U_{\mathrm{nn}}}{\partial Q_i} \end{aligned} \quad (11)$$

with the one-electron operator

$$\hat{v}_i^{(1)} = -\sum_\alpha \left[\frac{\partial}{\partial Q_i}\left(\frac{Z_\alpha e^2}{|\boldsymbol{r}_a - \boldsymbol{R}_\alpha|}\right)\right]_{\boldsymbol{R}_0}. \quad (12)$$

The indices a and α run over the electrons and nuclei, respectively, while Z_α refers to the charge of nucleus α, and e is the electronic charge. The nuclear repulsion term will be zero except for the normal modes with the totally symmetric representation.

Next, consider the benzene radical cation and anion. The $D_{6\mathrm{h}}$ equilibrium geometry of the neutral benzene molecule is used as the reference geometry R_0 throughout this work (Fig. 1). The benzene cation exhibits a degenerate ground electronic state in $D_{6\mathrm{h}}$ symmetry, with the degenerate $\psi_{e_{1\mathrm{g}}}$ orbitals not fully occupied. Similarly, the benzene anion has a degenerate ground electronic state because of its singly-occupied $\psi_{e_{2\mathrm{u}}}$ orbitals. As a result, both the benzene cation and anion will undergo a JT distortion, reducing the molecular symmetry to the $D_{2\mathrm{h}}$ point group.[89] We will use θ and ε throughout this work to distinguish between a degenerate pair of symmetry elements; see Fig. 2 as an example of this notation with the frontier orbitals of benzene.

We first consider the benzene cation, and denote $|E_{1\mathrm{g}}(\theta)\rangle$ and $|E_{1\mathrm{g}}(\varepsilon)\rangle$ as the degenerate electronic states of the cation which decompose to the $b_{2\mathrm{g}}$ and $b_{3\mathrm{g}}$ representations upon subduction of the molecular symmetry from $D_{6\mathrm{h}}$ to $D_{2\mathrm{h}}$. Under the space spanned by the degenerate $E_{1\mathrm{g}}$ electronic states of the

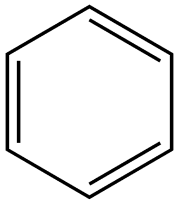

Fig. 1 The reference geometry used in this work; the B3LYP/def2-TZVPP optimised structure (C–C: 1.391 Å, C–H: 1.082 Å) of the neutral benzene molecule with a $D_{6\mathrm{h}}$ symmetry.

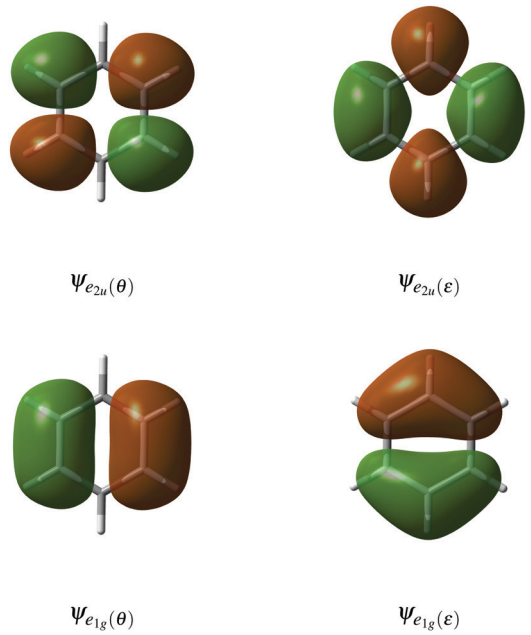

Fig. 2 Degenerate frontier orbitals of the neutral benzene molecule obtained with B3LYP/def2-TZVPP. Upon the subduction of the reference D_{6h} geometry of benzene to the D_{2h} point group, the irreducible representation of the highest occupied molecular orbitals (HOMOs) of benzene, $\psi_{e_{1g}(\theta)}$ and $\psi_{e_{1g}(\varepsilon)}$, will be reduced to b_{2g} and b_{3g} respectively, while the lowest unoccupied molecular orbitals (LUMOs) of benzene, $\psi_{e_{2u}(\theta)}$ and $\psi_{e_{2u}(\varepsilon)}$, are reduced to a_u and b_{1u} respectively.

cation, the linear vibronic coupling matrix ($\boldsymbol{V}_i^{(+,1)}$, in boldface) for normal mode i can be written as

$$\boldsymbol{V}_i^{(+,1)} = \begin{pmatrix} \left\langle E_{1g}(\theta)\middle|\hat{V}_i^{(1)}\middle|E_{1g}(\theta)\right\rangle & \left\langle E_{1g}(\theta)\middle|\hat{V}_i^{(1)}\middle|E_{1g}(\varepsilon)\right\rangle \\ \left\langle E_{1g}(\varepsilon)\middle|\hat{V}_i^{(1)}\middle|E_{1g}(\theta)\right\rangle & \left\langle E_{1g}(\varepsilon)\middle|\hat{V}_i^{(1)}\middle|E_{1g}(\varepsilon)\right\rangle \end{pmatrix}. \quad (13)$$

The + (−) sign in the superscript is used to denote the vibronic coupling matrix for the cation (anion), while the number refers to the order of the vibronic coupling matrix.

If the degenerate electronic states $|E_{1g}(\theta)\rangle$ and $|E_{1g}(\varepsilon)\rangle$ are both treated with single Slater determinants, the Slater–Condon rules for one-electron operators[90] can be applied to calculate the matrix elements of $\boldsymbol{V}_i^{(+,1)}$ as a sum of integrals over the occupied molecular orbitals.

First, the diagonal terms of $\boldsymbol{V}_i^{(+,1)}$ can be expressed as

$$\left\langle E_{1g}(\theta)\middle|\hat{V}_i^{(1)}\middle|E_{1g}(\theta)\right\rangle = \sum_m n_{m(\theta)}\left\langle \psi_m\middle|\hat{v}_i^{(1)}\middle|\psi_m\right\rangle + \frac{\partial U_{nn}}{\partial Q_i} \quad (14a)$$

$$\left\langle E_{1g}(\varepsilon)\middle|\hat{V}_i^{(1)}\middle|E_{1g}(\varepsilon)\right\rangle = \sum_m n_{m(\varepsilon)}\left\langle \psi_m\middle|\hat{v}_i^{(1)}\middle|\psi_m\right\rangle + \frac{\partial U_{nn}}{\partial Q_i} \quad (14b)$$

where m runs over the occupied orbitals of the benzene cation, and $n_{m(\theta)}$ and $n_{m(\varepsilon)}$ are the occupation numbers of the spatial orbital ψ_m in the Slater determinants corresponding to $|E_{1g}(\theta)\rangle$ and $|E_{1g}(\varepsilon)\rangle$, respectively. The off-diagonal terms are

$$\langle E_{1g}(\theta)|\hat{V}_i^{(1)}|E_{1g}(\varepsilon)\rangle = \langle E_{1g}(\varepsilon)|\hat{V}_i^{(1)}|E_{1g}(\theta)\rangle = \langle \psi_{e_{1g}(\varepsilon)}|\hat{v}_i^{(1)}|\psi_{e_{1g}(\theta)}\rangle = \langle \psi_{e_{1g}(\theta)}|\hat{v}_i^{(1)}|\psi_{e_{1g}(\varepsilon)}\rangle. \quad (15)$$

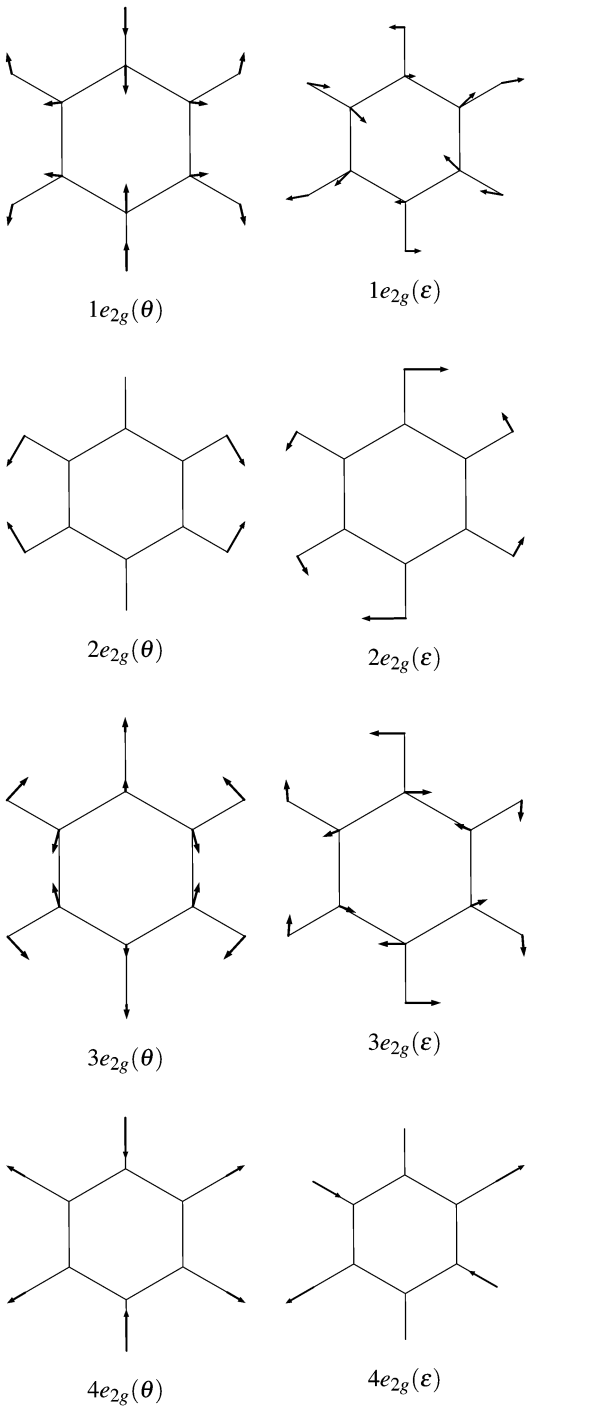

Fig. 3 B3LYP/def2-TZVPP e_{2g} normal modes of neutral benzene. Under the subduction $D_{6h} \rightarrow D_{2h}$, the e_{2g} representation is reduced to $a_{1g} \oplus b_{1g}$, and $e_{2g}(\theta)$ and $e_{2g}(\varepsilon)$ correspond to a_{1g} and b_{1g}, respectively.

The terms in eqn (14) and (15) are known as orbital vibronic coupling constants.[91,92]

The expressions for the matrix elements of $\boldsymbol{V}_i^{(+,1)}$ in eqn (14) and (15) can be simplified further using symmetry considerations. First, the symmetric product of the representations of the electronic states and normal mode i has to contain the totally symmetric representation for the matrix elements of $\boldsymbol{V}_i^{(+,1)}$ to be non-zero. This can be written as

$$A_{1g} \in E_{1g} \otimes E_{1g} \otimes \Gamma_i = \{A_{1g} \oplus E_{2g}\} \otimes \Gamma_i \quad (16)$$

where Γ_i is the symmetry representation of the normal mode i. Thus, the linear vibronic coupling matrices of the benzene cation will be non-zero only for normal modes with e_{2g} or a_{1g} symmetry.

For the e_{2g} normal modes of benzene (Fig. 3), the nuclear–nuclear repulsion term ($\partial U_{nn}/\partial Q_i$) is zero, while the orbital vibronic coupling constants corresponding to a molecular orbital ψ_m will be zero unless the product of the symmetry representation of ψ_m contains the E_{2g} representation:

$$E_{2g} \in \Gamma_m \otimes \Gamma_m \quad (17)$$

where Γ_m is the symmetry representation of the molecular orbital ψ_m.

Only molecular orbitals with the E_{1g}, E_{2g}, E_{1u}, and E_{2u} symmetries obey eqn (17), and have non-zero orbital vibronic coupling constants. By the Wigner–Eckart theorem,[93] the magnitude of the orbital vibronic coupling constants for a degenerate pair of molecular orbitals is equal to each other. Because of the opposing signs in the respective Clebsch–Gordan coefficients,[94] the orbital vibronic coupling constants of a degenerate pair of molecular orbitals will cancel each other out:

$$\left\langle \psi_{m(\theta)} \middle| \hat{v}_{e_{2g}}^{(1)} \middle| \psi_{m(\theta)} \right\rangle + \left\langle \psi_{m(\varepsilon)} \middle| \hat{v}_{e_{2g}}^{(1)} \middle| \psi_{m(\varepsilon)} \right\rangle = 0 \quad (18)$$

for m in e_{1g}, e_{2g}, e_{1u}, and e_{2u}. As a result, only the doubly occupied frontier orbitals in the benzene cation contribute to the summation in eqn (14).

Thus, the diagonal elements of $\boldsymbol{V}_i^{(+,1)}$ in eqn (14) can be further reduced to

$$\begin{aligned}
\left\langle E_{1g}(\theta) \middle| \hat{V}_{e_{2g}}^{(1)} \middle| E_{1g}(\theta) \right\rangle &= \sum_m n_{m(\theta)} \left\langle \psi_m \middle| \hat{v}_{e_{2g}}^{(1)} \middle| \psi_m \right\rangle \\
&= \sum_{m \in \{e_{2g}, e_{1u}, e_{2u}\}} n_{m(\theta)} \left\langle \psi_m \middle| \hat{v}_{e_{2g}}^{(1)} \middle| \psi_m \right\rangle \\
&\quad + \left\langle \psi_{e_{1g}(\theta)} \middle| \hat{v}_{e_{2g}}^{(1)} \middle| \psi_{e_{1g}(\theta)} \right\rangle \\
&\quad + 2 \left\langle \psi_{e_{1g}(\varepsilon)} \middle| \hat{v}_{e_{2g}}^{(1)} \middle| \psi_{e_{1g}(\varepsilon)} \right\rangle \\
&= \left\langle \psi_{e_{1g}(\varepsilon)} \middle| \hat{v}_{e_{2g}}^{(1)} \middle| \psi_{e_{1g}(\varepsilon)} \right\rangle
\end{aligned} \quad (19a)$$

$$\begin{aligned}
\left\langle E_{1g}(\varepsilon) \middle| \hat{V}_{e_{2g}}^{(1)} \middle| E_{1g}(\varepsilon) \right\rangle &= \sum_m n_{m(\varepsilon)} \left\langle \psi_m \middle| \hat{v}_{e_{2g}}^{(1)} \middle| \psi_m \right\rangle \\
&= \sum_{m \in \{e_{2g}, e_{1u}, e_{2u}\}} n_{m(\varepsilon)} \left\langle \psi_m \middle| \hat{v}_{e_{2g}}^{(1)} \middle| \psi_m \right\rangle \\
&\quad + 2 \left\langle \psi_{e_{1g}(\theta)} \middle| \hat{v}_{e_{2g}}^{(1)} \middle| \psi_{e_{1g}(\theta)} \right\rangle \\
&\quad + \left\langle \psi_{e_{1g}(\varepsilon)} \middle| \hat{v}_{e_{2g}}^{(1)} \middle| \psi_{e_{1g}(\varepsilon)} \right\rangle \\
&= \left\langle \psi_{e_{1g}(\theta)} \middle| \hat{v}_{e_{2g}}^{(1)} \middle| \psi_{e_{1g}(\theta)} \right\rangle
\end{aligned} \quad (19b)$$

Hence, the linear vibronic coupling matrix $\boldsymbol{V}_{e_{2g}}^{(+,1)}$ for the e_{2g} normal modes of the benzene cation can be written in terms of orbital vibronic coupling constants as:

$$\boldsymbol{V}_{e_{2g}}^{(+,1)} = \begin{pmatrix} \left\langle \psi_{e_{1g}(\varepsilon)} \middle| \hat{v}_{e_{2g}}^{(1)} \middle| \psi_{e_{1g}(\varepsilon)} \right\rangle & \left\langle \psi_{e_{1g}(\varepsilon)} \middle| \hat{v}_{e_{2g}}^{(1)} \middle| \psi_{e_{1g}(\theta)} \right\rangle \\ \left\langle \psi_{e_{1g}(\theta)} \middle| \hat{v}_{e_{2g}}^{(1)} \middle| \psi_{e_{1g}(\varepsilon)} \right\rangle & \left\langle \psi_{e_{1g}(\theta)} \middle| \hat{v}_{e_{2g}}^{(1)} \middle| \psi_{e_{1g}(\theta)} \right\rangle \end{pmatrix}. \quad (20)$$

According to the Wigner–Eckart theorem, the vibronic coupling matrix for a degenerate pair of e_{2g} normal modes ($\nu_{e_{2g}(\theta)}$ and $\nu_{e_{2g}(\varepsilon)}$) can be reduced as

$$\begin{aligned}
\boldsymbol{V}_{e_{2g}(\theta)}^{(+,1)} &= \frac{1}{\sqrt{2}} \left\langle E_{1g} \middle\| \hat{V}_{e_{2g}}^{(1)} \middle\| E_{1g} \right\rangle \begin{pmatrix} \frac{1}{\sqrt{2}} & 0 \\ 0 & -\frac{1}{\sqrt{2}} \end{pmatrix} \\
&= \frac{1}{2} \left\langle E_{1g} \middle\| \hat{V}_{e_{2g}}^{(1)} \middle\| E_{1g} \right\rangle \begin{pmatrix} 1 & 0 \\ 0 & -1 \end{pmatrix}
\end{aligned} \quad (21a)$$

$$\begin{aligned}
\boldsymbol{V}_{e_{2g}(\varepsilon)}^{(+,1)} &= \frac{1}{\sqrt{2}} \left\langle E_{1g} \middle\| \hat{V}_{e_{2g}}^{(1)} \middle\| E_{1g} \right\rangle \begin{pmatrix} 0 & \frac{1}{\sqrt{2}} \\ \frac{1}{\sqrt{2}} & 0 \end{pmatrix} \\
&= \frac{1}{2} \left\langle E_{1g} \middle\| \hat{V}_{e_{2g}}^{(1)} \middle\| E_{1g} \right\rangle \begin{pmatrix} 0 & 1 \\ 1 & 0 \end{pmatrix}
\end{aligned} \quad (21b)$$

where $\left\langle E_{1g} \middle\| \hat{V}_{e_{2g}}^{(1)} \middle\| E_{1g} \right\rangle$ is the reduced matrix element.

Thus, a single vibronic coupling constant $V_{e_{2g}}^{(+,1)}$ is sufficient to describe the linear vibronic coupling for a degenerate pair of e_{2g} normal modes in the benzene cation, and can be calculated as the orbital vibronic coupling constants of its frontier HOMOs:

$$\begin{aligned}
V_{e_{2g}}^{(+,1)} &= \frac{1}{2} \left\langle E_{1g} \middle\| \hat{V}_{e_{2g}}^{(1)} \middle\| E_{1g} \right\rangle \\
&= \left\langle \psi_{e_{1g}(\varepsilon)} \middle| \hat{v}_{e_{2g}(\theta)}^{(1)} \middle| \psi_{e_{1g}(\varepsilon)} \right\rangle \\
&= -\left\langle \psi_{e_{1g}(\theta)} \middle| \hat{v}_{e_{2g}(\theta)}^{(1)} \middle| \psi_{e_{1g}(\theta)} \right\rangle \\
&= \left\langle \psi_{e_{1g}(\theta)} \middle| \hat{v}_{e_{2g}(\varepsilon)}^{(1)} \middle| \psi_{e_{1g}(\varepsilon)} \right\rangle
\end{aligned} \quad (22)$$

Computationally, the electronic degeneracy in an open-shell radical system would typically preclude the usage of single

configuration methods such as DFT on the benzene cation directly.[87,95] To avoid the problem of degeneracy, we will derive the vibronic coupling constants of the benzene cation using the orbital vibronic coupling constants of the closed-shell neutral benzene molecule instead. As the orbitals of interest are the degenerate HOMOs of the highly symmetric benzene molecule, the addition or removal of an electron should not affect these π-orbitals, and hence the calculated orbital vibronic coupling constants significantly. This approach was used in our previous study on the JT distortion in the cyclopentadienyl radical,[47] and we hope to further validate it here.

Next, we consider the a_{1g} normal modes (Fig. 4). Using eqn (13), the linear vibronic coupling matrix for the a_{1g} normal modes can be written as

$$\boldsymbol{V}^{(+,1)}_{a_{1g}} = \begin{pmatrix} \left\langle E_{1g}(\theta)\middle|\hat{V}^{(1)}_{a_{1g}}\middle|E_{1g}(\theta)\right\rangle & 0 \\ 0 & \left\langle E_{1g}(\varepsilon)\middle|\hat{V}^{(1)}_{a_{1g}}\middle|E_{1g}(\varepsilon)\right\rangle \end{pmatrix}. \tag{23}$$

The off-diagonal elements of the vibronic coupling matrix for the a_{1g} normal modes are zero by symmetry considerations, and the diagonal matrix elements are yet to be calculated.

To do so, we extend the neglect of orbital relaxation beyond the degenerate HOMOs to include all occupied orbitals in the benzene radical cation. In other words, the occupied orbitals in the benzene radical cation are all treated with the corresponding orbitals in the neutral benzene molecule.

The diagonal matrix elements can then be calculated with reference to the vibronic coupling constants of the neutral benzene molecule. These are just the force constants of neutral benzene, which is zero at the optimised equilibrium geometry.

$$\left\langle \Psi_0\middle|\hat{V}^{(1)}_i\middle|\Psi_0\right\rangle = \sum_{m'} n_{m'}\left\langle \psi_{m'}\middle|\hat{v}^{(1)}_i\middle|\psi_{m'}\right\rangle + \frac{\partial U_{nn}}{\partial Q_i} = 0, \tag{24}$$

where Ψ_0 is the ground electronic state of neutral benzene, $n_{m'}$ is the occupation number of molecular orbital $\psi_{m'}$ in Ψ_0.

If all orbital relaxation effects are ignored, the orbitals for the cation and neutral molecule are equal, *i.e.* $\psi_m = \psi_{m'}$. Using eqn (14), the diagonal matrix elements can then be calculated as

$$\begin{aligned}\left\langle E_{1g}(\theta)\middle|\hat{V}^{(1)}_{a_{1g}}\middle|E_{1g}(\theta)\right\rangle &= \sum_m n_{m(\theta)}\left\langle \psi_m\middle|\hat{v}^{(1)}_{a_{1g}}\middle|\psi_m\right\rangle + \frac{\partial U_{nn}}{\partial Q_{a_{1g}}} \\ &= \sum_{m'} n_{m'}\left\langle \psi_{m'}\middle|\hat{v}^{(1)}_{a_{1g}}\middle|\psi_{m'}\right\rangle + \frac{\partial U_{nn}}{\partial Q_{a_{1g}}} \\ &\quad -\left\langle \psi_{e_{1g}(\theta)}\middle|\hat{v}^{(1)}_{a_{1g}}\middle|\psi_{e_{1g}(\theta)}\right\rangle \\ &= -\left\langle \psi_{e_{1g}(\theta)}\middle|\hat{v}^{(1)}_{a_{1g}}\middle|\psi_{e_{1g}(\theta)}\right\rangle\end{aligned} \tag{25a}$$

$$\begin{aligned}\left\langle E_{1g}(\varepsilon)\middle|\hat{V}^{(1)}_{a_{1g}}\middle|E_{1g}(\varepsilon)\right\rangle &= \sum_m n_m\left\langle \psi_m\middle|\hat{v}^{(1)}_{a_{1g}}\middle|\psi_m\right\rangle + \frac{\partial U_{nn}}{\partial Q_{a_{1g}}} \\ &= \sum_{m'} n_{m'}\left\langle \psi_{m'}\middle|\hat{v}^{(1)}_{a_{1g}}\middle|\psi_{m'}\right\rangle + \frac{\partial U_{nn}}{\partial Q_{a_{1g}}} \\ &\quad -\left\langle \psi_{e_{1g}(\varepsilon)}\middle|\hat{v}^{(1)}_{a_{1g}}\middle|\psi_{e_{1g}(\varepsilon)}\right\rangle \\ &= -\left\langle \psi_{e_{1g}(\varepsilon)}\middle|\hat{v}^{(1)}_{a_{1g}}\middle|\psi_{e_{1g}(\varepsilon)}\right\rangle\end{aligned} \tag{25b}$$

According to the Wigner–Eckart theorem, $\left\langle E_{1g}(\theta)\middle|\hat{V}^{(1)}_{a_{1g}}\middle|E_{1g}(\theta)\right\rangle$ and $\left\langle E_{1g}(\varepsilon)\middle|\hat{V}^{(1)}_{a_{1g}}\middle|E_{1g}(\varepsilon)\right\rangle$ are equal. Thus, the vibronic coupling constant $V^{(+,1)}_{a_{1g}}$ for the a_{1g} normal modes can be calculated in terms of orbital vibronic coupling constants as:

$$\begin{aligned}V^{(+,1)}_{a_{1g}} &= -\left\langle \psi_{e_{1g}(\theta)}\middle|\hat{v}^{(1)}_{a_{1g}}\middle|\psi_{e_{1g}(\theta)}\right\rangle \\ &= -\left\langle \psi_{e_{1g}(\varepsilon)}\middle|\hat{v}^{(1)}_{a_{1g}}\middle|\psi_{e_{1g}(\varepsilon)}\right\rangle\end{aligned} \tag{26}$$

Lastly, we consider the benzene radical anion. Using the symmetries of the LUMOs in neutral benzene (Fig. 2), the degenerate electronic states of the benzene anion are denoted as $|E_{2u}(\theta)\rangle$ and $|E_{2u}(\varepsilon)\rangle$. The selection rule for determining which normal modes i are linear JT active is

$$A_{1g} \in E_{2u} \otimes E_{2u} \otimes \Gamma_i = \{A_{1g} \oplus E_{2g}\} \otimes \Gamma_i \tag{27}$$

which is the same result as that of the benzene cation (eqn (16)).

Hence, the derivation of the vibronic coupling constants for the benzene anion in terms of orbital vibronic coupling constants follows that of the benzene cation, and is omitted for brevity. The final result, the linear vibronic coupling constants for the benzene anion, $V^{(-,1)}_{e_{1g}}$ and $V^{(-,1)}_{a_{1g}}$, can be expressed in terms of orbital vibronic coupling constants as

$$\begin{aligned}V^{(-,1)}_{e_{1g}} &= \left\langle E_{2u}(\theta)\middle|\hat{V}^{(1)}_{e_{2g}}\middle|E_{2u}(\theta)\right\rangle \\ &= \left\langle \psi_{e_{2u}(\theta)}\middle|\hat{v}^{(1)}_{e_{2g}}\middle|\psi_{e_{2u}(\theta)}\right\rangle \\ &= -\left\langle \psi_{e_{2u}(\varepsilon)}\middle|\hat{v}^{(1)}_{e_{2g}}\middle|\psi_{e_{2u}(\varepsilon)}\right\rangle \\ &= \left\langle \psi_{e_{2u}(\theta)}\middle|\hat{v}^{(1)}_{e_{2g}}\middle|\psi_{e_{2u}(\varepsilon)}\right\rangle\end{aligned} \tag{28}$$

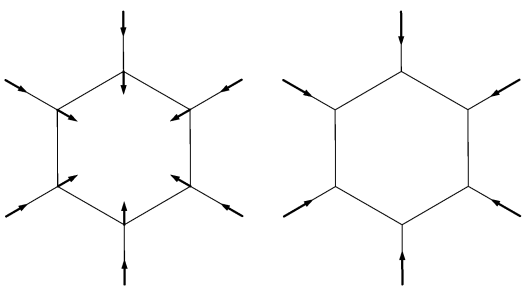

Fig. 4 B3LYP/def2-TZVPP a_{1g} normal modes of neutral benzene.

$$\begin{aligned} V_{a_{1g}}^{(-,1)} &= \left\langle E_{2u}(\theta)\middle|\hat{V}_{a_{1g}}^{(1)}\middle|E_{2u}(\theta)\right\rangle \\ &= \left\langle \psi_{e_{2u}(\theta)}\middle|\hat{v}_{a_{1g}}^{(1)}\middle|\psi_{e_{2u}(\theta)}\right\rangle \\ &= \left\langle \psi_{e_{2u}(\varepsilon)}\middle|\hat{v}_{a_{1g}}^{(1)}\middle|\psi_{e_{2u}(\varepsilon)}\right\rangle. \end{aligned} \tag{29}$$

The orbital vibronic coupling constants in eqn (28) and (29) will also be calculated using the degenerate LUMOs of neutral benzene.

Summarising this section, the vibronic coupling constants of the benzene radical cation and anion have been reduced to the orbital vibronic coupling constants of their respective frontier orbitals. The orbital vibronic coupling constants will be calculated as the gradient of the Kohn–Sham orbitals of the neutral benzene molecule to avoid the problem of degeneracy. In the case of *GW*, the energy gradient of the quasiparticle representing the ionization or addition of an electron to the respective frontier orbitals of benzene will be used to calculate the vibronic coupling constants of the benzene radical cation.

2.2 *GW* approximation

A brief overview of the *GW*-based methods used in this work is given in this section.[27,28,32] Within many-body perturbation theory, the quasiparticle representing the addition or removal of an electron to a system can be characterised using the time-ordered Green's function.[29] The time-ordered Green's function G for an interacting system obeys the Dyson equation,

$$G(\mathbf{1},\mathbf{2}) = G_{\text{non-int.}}(\mathbf{1},\mathbf{2}) + \int d(\mathbf{34}) G_{\text{non-int.}}(\mathbf{1},\mathbf{3})\Sigma(\mathbf{3},\mathbf{4})G(\mathbf{4},\mathbf{2}), \tag{30}$$

where $G_{\text{non-int.}}$ is the Green's function for a non-interacting system, Σ is the self-energy, and the notation $\mathbf{1} = (r_1, t_1)$ is used to represent the spatial and time coordinates.

However, the exact self-energy is not known, and has to be approximated. Hedin's approach was to expand the self-energy in terms of the screened Coulomb interaction W,[30]

$$\Sigma(\mathbf{1},\mathbf{2}) = i\int d(\mathbf{34}) G(\mathbf{1},\mathbf{3}) W(\mathbf{1},\mathbf{4}) \Gamma(\mathbf{3},\mathbf{2},\mathbf{4}) \tag{31}$$

with W calculated using the bare Coulomb potential $V(r_1, r_2) = e^2/|r_1 - r_2|$ and a polarisability term P

$$W(\mathbf{1},\mathbf{2}) = V(\mathbf{1},\mathbf{2}) + \int d(\mathbf{34}) V(\mathbf{1},\mathbf{3}) P(\mathbf{3},\mathbf{4}) W(\mathbf{4},\mathbf{2}) \tag{32}$$

$$P(\mathbf{1},\mathbf{2}) = -i\int d(\mathbf{34}) G(\mathbf{4},\mathbf{2}) G(\mathbf{2},\mathbf{3}) \Gamma(\mathbf{3},\mathbf{4},\mathbf{1}), \tag{33}$$

and the vertex function Γ,

$$\begin{aligned} \Gamma(\mathbf{1},\mathbf{2},\mathbf{3}) &= \delta(\mathbf{1},\mathbf{2})\delta(\mathbf{2},\mathbf{3}) \\ &+ \int d(\mathbf{4567}) \frac{\delta\Sigma(\mathbf{1},\mathbf{2})}{\delta G(\mathbf{4},\mathbf{5})} G(\mathbf{4},\mathbf{6}) G(\mathbf{7},\mathbf{5}) \Gamma(\mathbf{6},\mathbf{7},\mathbf{3}). \end{aligned} \tag{34}$$

Eqn (30)–(34) are known as Hedin's equations.[30] To further simplify the problem, the vertex correction is neglected; *i.e.*, the second term of eqn (34) is ignored. The self-energy in eqn (31) becomes $\Sigma = iGW$, and the polarisability $P = -iGG$.

Using the random-phase approximation, the screened Coulomb interaction can be expressed in terms of an dynamical dielectric function ε^{-1},

$$W(\mathbf{1},\mathbf{2}) = \int d(\mathbf{3}) \varepsilon^{-1}(\mathbf{1},\mathbf{3}) V(\mathbf{3},\mathbf{2}), \tag{35}$$

where ε is obtained by treating the density response function with the polarisability P,

$$\varepsilon(\mathbf{1},\mathbf{2}) = \delta(\mathbf{1},\mathbf{2}) - \int d(\mathbf{3}) V(\mathbf{1},\mathbf{3}) P(\mathbf{3},\mathbf{2}). \tag{36}$$

Finally, $G_{\text{non-int.}}$ can be approximated by the one-particle Green's function for electrons in a mean-field system. The spectral representation of $G_{\text{non-int.}}$ is then

$$G_{\text{non-int}}(r_1, r_2, \xi) = \sum_i \frac{\psi_i(r_1)\psi_i(r_2)}{\xi - \varepsilon_i - i\eta} + \sum_a \frac{\psi_a(r_1)\psi_a(r_2)}{\xi - \varepsilon_a + i\eta} \tag{37}$$

where ε and ψ are the one-electron eigenvalues and eigenstates, respectively, the indices i and a refer to the occupied and unoccupied orbitals, respectively, and η is a positive infinitesimal.

In principle, using eqn (37) as a starting point, Hedin's equations simplified with the *GW* approximation can be solved self-consistently to obtain the Green's function for an interacting system. However, this remains a challenging task, and requires further approximations to be computationally practical.

To start, consider the quasiparticle equation, a one-particle eigenvalue problem which can be derived from the Dyson equation for G (eqn (30)):

$$\left(-\frac{\nabla^2}{2} + V_{\text{ext.}} + V_{\text{Har.}} + \int \mathrm{d}r' \Sigma^{GW}\left(r, r', \varepsilon_i^{\text{QP}}\right)\right)\psi_i^{\text{QP}}(r) = \varepsilon_i^{\text{QP}}\psi_i^{\text{QP}}(r) \tag{38}$$

where the self-energy operator $\Sigma^{GW}(r, r', \varepsilon_i^{\text{QP}})$, which is in general complex and non-Hermitian, is used to describe exchange and correlation. The solutions of the quasiparticle equation are then the quasiparticle energies $\varepsilon_i^{\text{QP}}$ and wave functions ψ_i^{QP}.

In the 'one-shot' G_0W_0 method, the quasiparticle wave functions are approximated by the one-electron wave functions of a mean-field Hamiltonian, such as HF or Kohn–Sham DFT. The quasiparticle energies can then be obtained by the perturbative correction to the eigenvalues of the mean-field result,

$$\varepsilon_i^{\text{QP}} = \varepsilon_i + \left\langle \Psi_i\middle|\Sigma\left(\varepsilon_i^{\text{QP}}\right) - V_{\text{XC}}\middle|\Psi_i\right\rangle. \tag{39}$$

Eqn (39) can be solved graphically or linearised by expanding the self-energy about the mean-field eigenvalues:

$$\varepsilon_i^{\text{QP}} = \varepsilon_i + Z_i\langle\Psi_i|\Sigma(\varepsilon_i) - V_{\text{XC}}|\Psi_i\rangle \tag{40}$$

using the renormalisation factor Z_i

$$Z_i = \left(1 - \left(\frac{\mathrm{d}\Sigma(\xi)}{\mathrm{d}\xi}\right)_{\xi=\varepsilon_i}\right)^{-1}. \tag{41}$$

Summing up, the G_0W_0 method starts with a mean-field calculation and carries out a single iteration of Hedin's equations.

In eigenvalue self-consistent *GW* (ev*GW*), the updated quasiparticle energies are re-entered into the computation of the Green's function in eqn (37) after G_0W_0 calculation. The re-calculation of W and Σ follows, and leads to a further correction to the quasiparticle energies. This process is iterated until self-consistency in the quasiparticle energies is achieved, while the quasiparticle wave function is treated with the mean-field wave function throughout. A simplification to the above would be to perform self-consistency only in the calculation of G, *i.e.*, W is not updated after the first G_0W_0 calculation (evGW_0).

Next, the quasiparticle self-consistent *GW* method, qs*GW*, updates both the quasiparticle wave function and energies with each iteration. To do so, a static and Hermitian approximation to the *GW* self-energy is used such that the matrix elements of the self-energy operator in qs*GW* becomes

$$\left\langle \psi_i \middle| \Sigma^{\mathrm{qs}GW} \middle| \psi_j \right\rangle = \frac{1}{2}\left[\mathrm{Re}\left\langle \psi_i \middle| \Sigma^{GW}(\varepsilon_i) + \Sigma^{GW}(\varepsilon_j) \middle| \psi_j \right\rangle \right] \quad (42)$$

where 'Re' refers to the Hermitian part of Σ^{GW}. Replacing Σ^{GW} by $\Sigma^{\mathrm{qs}GW}$ in eqn (38) ensures the Hermiticity of the quasiparticle equation, and allows it to be solved self-consistently to obtain the quasiparticle energies within qs*GW*.

3 Computational details

The optimised D_{6h} geometry (Fig. 1) and vibrational normal modes (Table 1) of neutral benzene were first obtained at the B3LYP/def2-TZVPP[96–98] level of theory using Gaussian16.[99]

Next, the molgw v2.D program[100] was used to obtain the Kohn–Sham orbital energies and *GW* quasiparticle energies corresponding to the degenerate HOMOs and LUMOs of the neutral benzene molecule with respect to distortions along the individual a_{1g} and e_{2g} normal modes (Fig. 3 and 4).

A polynomial fit was then used to obtain the derivatives of the respective energies (Fig. 5 and ESI†). The same procedure was also used to obtain the molecular vibrational frequencies as the second derivatives of the total energies within the various exchange–correlation functionals used in this work, which includes the standard BLYP,[101,102] B3LYP, CAM-B3LYP,[103] and tuned CAM-B3LYP (tCAM-B3LYP)[104] functionals.

Table 1 Harmonic vibrational frequencies ω_i (cm^{-1}) of benzene at the B3LYP/def2-TZVPP level of theory

ν_i	Frequency, ω_i	ν_i	Frequency, ω_i
$1a_{1g}$	1015	$1a_{2u}$	691
$2a_{1g}$	3196	$1b_{1u}$	1030
$1a_{2g}$	1389	$2b_{1u}$	3161
$1b_{2g}$	725	$1b_{2u}$	1176
$2b_{2g}$	1020	$2b_{2u}$	1336
$1e_{1g}$	868	$1e_{1u}$	1062
$1e_{2g}$	624	$2e_{1u}$	1519
$2e_{2g}$	1200	$3e_{1u}$	3186
$3e_{2g}$	1637	$1e_{2u}$	414
$4e_{2g}$	3170	$2e_{2u}$	989

In addition, a number of studies have tested the use of IP-tuned functionals in conjunction with the *GW* methods, and have found that the IP-tuning of the range-separation parameters leads to an improvement in the DFT and G_0W_0 results.[33,43–45,105] As a result, the IP-tuning procedure was also applied to the tuned CAM-B3LYP functional by Okuno *et al.*, which is then denoted as IP-tCAM-B3LYP in this work. Details of the IP-tuning are given in the ESI.†

The *GW* methods (G_0W_0, evGW_0, ev*GW*, and qs*GW*) were then applied on top of each exchange–correlation functional separately. The evGW_0 and ev*GW* calculations were iterated until the quasiparticle energies corresponding to the degenerate HOMOs and LUMOs converged to within 0.005 eV of the previous iteration. Unless otherwise stated, all calculations in this work were carried out with the def2-TZVPP basis set.[98] All molgw v2.D calculations were carried out with the resolution-of-identity approximation[106] and the frozen core approximation for *GW* calculations.[37]

4 Results and discussion

4.1 Ionization potential and electron affinity of benzene

We start our discussion of the results by looking at the electronic properties of benzene, and the degenerate HOMOs and LUMOs of neutral benzene in particular. These frontier molecular orbitals can in turn be related to the vertical IP and electron affinity (EA) using a Koopmans' theorem-like approach.[3] Ideally, experimental values for the vertical IP and EA of benzene would be used to benchmark the DFT and *GW* methods used in this work.[107] However, experimental measurements are complicated by the presence of intrinsic effects such as zero-point vibrational energies, as well as possible uncertainties as to whether the experimentally measured IP and EA are vertical or adiabatic.[72,80] Hence, we will benchmark our results against computational CCSD(T) values from the literature.[44]

The errors in the vertical IP and EA of neutral benzene calculated using DFT, G_0W_0, evGW_0, ev*GW*, and qs*GW* with respect to CCSD(T) values are given in Fig. 6. Because the basis set effect on the *GW* quasiparticle energies is known to be large,[31,37,38,44,108–110] we also calculated the vertical IPs and EAs with the def2-QZVPP basis set.[98] The difference between the *GW* values for def2-TZVPP and def2-QZVPP was found to be quite large, about 0.2–0.3 eV, and shows the importance of the basis set effect (ESI†). As a result, the def2-QZVPP values will be used for the following discussion of the vertical IP and EA of benzene.

Benzene, being a prototypical aromatic molecule, has been investigated in numerous studies of the *GW* approximation.[31,32,34,38,44,109–111] Our results follow the trends observed in the earlier studies, and are summarised below.

In general, there is no notable difference between the accuracies of the computed IP and EA within a single method. The IP and EA calculated using DFT with standard functionals is largely poor. On the other hand, the results for the IP-tuned CAM-B3LYP functional (IP-tCAM-B3LYP) is excellent, with the

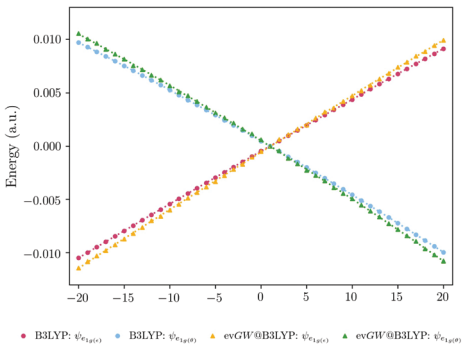

Fig. 5 B3LYP Kohn–Sham orbital and ev*GW*@B3LYP quasiparticle energies for the degenerate HOMOs of neutral benzene with respect to a distortion along the $3e_{2g}(\theta)$ normal mode. The energies were vertically shifted to set the energies at R_0 to be zero.

computed IP and EA within 0.05 eV of the CCSD(T) values. Hence, the considerable improvement in the calculated IP and EA supports the use of IP-tuning to redefine the parameters of standard DFT functionals in a molecule-specific manner.

Next, the perturbative G_0W_0 correction leads to a vast improvement in the initial DFT results, albeit the dependence on the DFT starting point remains substantial. The errors in G_0W_0@BLYP and G_0W_0@B3LYP are still quite large, at about 0.3 to 0.4 eV, while the error for G_0W_0 with the two standard range-separated functionals (CAM-B3LYP and tCAM-B3LYP) is significantly smaller at about 0.1 eV to the CCSD(T) values. The accuracy of the DFT result for IP-tCAM-B3LYP means that the effect of the G_0W_0 correction is minimal.

The starting point dependence is reduced further in evGW_0, and is almost completely eliminated in ev*GW*. This is accompanied by an improvement in the calculated IP and EA, with the errors in the ev*GW* results falling below 0.05 eV for all five functionals. Lastly, as the quasiparticle wave function is obtained self-consistently in qs*GW*, the resulting IP and EA are completely independent of the DFT starting point, and are comparable to ev*GW* in terms of the accuracy.

Thus, we can conclude that *GW* approximation is capable of modelling the electronic properties of benzene accurately. The limitations of DFT are already strongly alleviated with the simplest G_0W_0 approach, with further improvements observed upon the introduction of self-consistency. More specifically, ev*GW* and qs*GW* provide excellent results for both IP and EA regardless of the DFT starting point, while G_0W_0 can only yield accurate IPs and EAs when used with long-range corrected functionals. It is worth noting that the IP-tuned CAM-B3LYP can match the ev*GW* results, and only requires DFT calculations in terms of the computational cost.

4.2 Vibrational properties of neutral benzene

After the electronic properties of benzene, we examine the other component of vibronic coupling, the vibrational motion. The effect of the basis set and normal mode coordinates used in the numerical calculation of the vibrational frequencies was found to be weak in our earlier study of the cyclopentadienyl radical,[47] and we confirm it again here. We also explored the

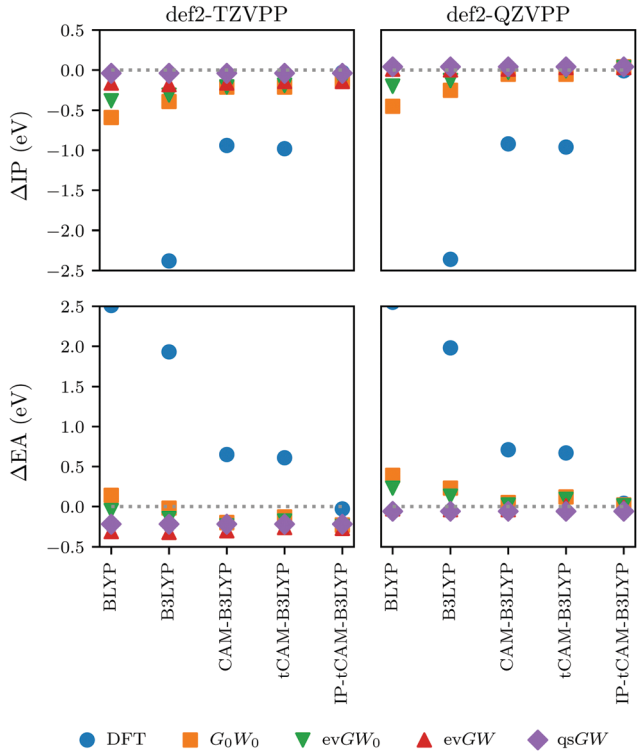

Fig. 6 Comparison between the vertical IP (ΔIP) and EA (ΔEA) of benzene within DFT and *GW* to CCSD(T) values extrapolated to the complete basis set limit.[44] The results obtained using the def2-TZVPP and def2-QZVPP basis sets are both given. The DFT results for BLYP are partially cut off because of the size in the errors. The full set of numerical results is given in the ESI.†

use of the Galitski–Migdal formula[112] with the Green's function from a G_0W_0 calculation to obtain the total molecular energies. The vibrational frequencies within *GW* were then obtained as the second derivative of the total energies with respect to the a_{1g} and e_{2g} normal modes. The full set of numerical results is given in the ESI.†

As in the previous section, we will compare the obtained vibrational frequencies to the CCSD(T) values from the literature[113] (Fig. 7). Unlike the results for IP and EA, no single method or functional clearly outperforms the rest. The quality of the DFT and *GW* vibrational frequencies is comparable to each other for the $1e_{2g}$, $2e_{2g}$, and $3e_{2g}$ normal modes, while that of DFT is slightly better for the $1a_{1g}$, $2a_{1g}$, and $4e_{2g}$ normal modes.

The use of the Galitski–Migdal total energies to model the a_{1g} and e_{2g} normal modes within *GW* does not appear to be an improvement upon DFT. The performance of the various functionals within DFT is also mostly similar to each other, with the largest disparity found in the C–H bond stretching ($2a_{1g}$ and $4e_{2g}$) modes. The performance of the three range-separated functionals for these two normal modes is poorer compared to those of BLYP and B3LYP.

Before proceeding to the discussion on vibronic coupling constants, we note that we will use the vibrational frequencies of neutral benzene to treat the benzene radical cation and

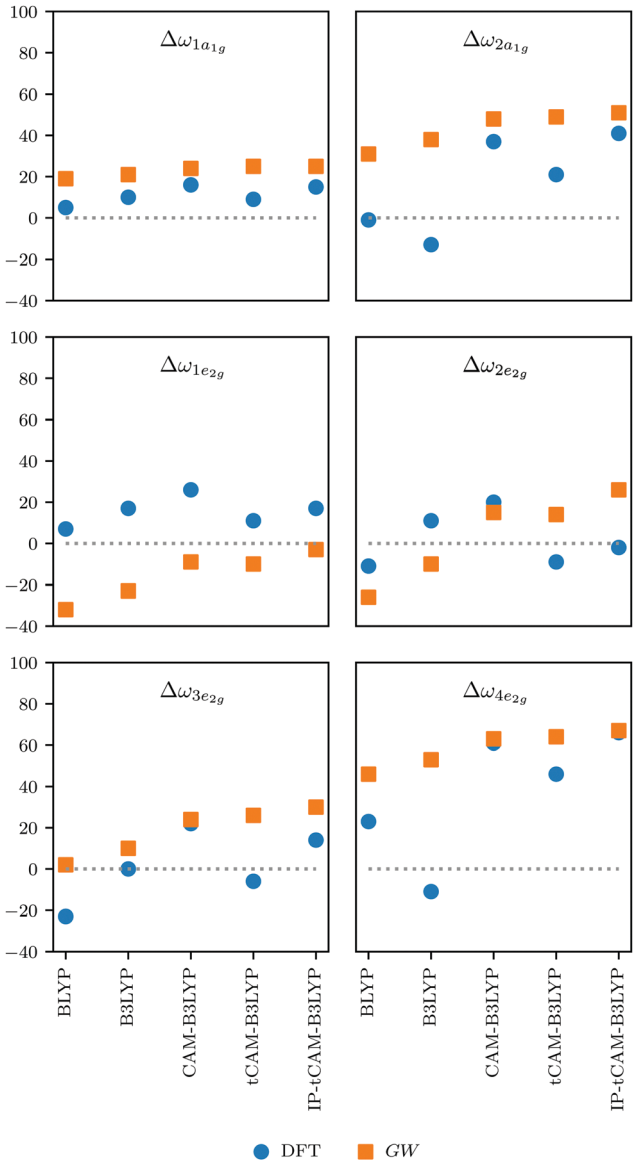

Fig. 7 Comparison of the vibrational frequencies of the a_{1g} and e_{2g} normal modes obtained within DFT and *GW* to the CCSD(T)/cc-pVTZ values.[113] The difference to CCSD(T) values ($\Delta\omega_i$) is given in cm^{-1}.

anion. Essentially, the reduction of the linear vibronic coupling constants of the benzene radical cation and anion to a single orbital vibronic coupling constant is discussed in Section 2.1 above. This approach can be extended to treat the vibrational frequencies of the radical cation and anion as the difference between the corresponding vibrational frequencies of the neutral molecule and the second derivatives of the orbital energies. As the second derivatives of the orbital energies for the frontier orbitals of benzene were found to be small, it will be sufficient to use the vibrational frequencies of neutral benzene for the radical cation and anion. Further details on the derivation and the computational results are given in the ESI.† Because of their slightly superior accuracy, the DFT vibrational frequencies will be used for the calculation of the dimensionless vibronic coupling constants.

4.3 Linear vibronic coupling constants

As stated in the Introduction, the aim of the present study is to investigate the computation of vibronic coupling constants using approximate self-consistent *GW* methods. There are two main points to consider towards this end: the starting point dependence of these methods and the accuracy of the computed results.

We examine the first question by looking at $V_i^{(+,1)}$ and $V_i^{(-,1)}$ for the benzene radical cation and anion. The DFT and *GW* results are given in Fig. 8, 9 and the ESI.† We will use a simplified notation without superscripts, V_i, to refer to both $V_i^{(+,1)}$ and $V_i^{(-,1)}$ simultaneously.

As observed in our previous work,[47] the dependence of the DFT results on the exchange–correlation functional is a lot weaker compared to the IP and EA of benzene discussed earlier. The DFT results lie within 0.5×10^{-4} a.u. of each other, except for $V_{3e_{2g}}^{(+,1)}$.

The variance in the results is further reduced in G_0W_0, and the introduction of self-consistency within *GW* leads to a further agreement across the five functionals. Other than $V_{2a_{1g}}^{(+,1)}$, the qs*GW* and ev*GW* values are about 0.1×10^{-4} a.u. of each other. Therefore, we confirm that the use of approximate self-consistent *GW* methods removes the starting point dependence in the computed vibronic coupling constants.

Because of its performance for the IP and EA, the DFT results for the IP-tCAM-B3LYP functional is also of interest.

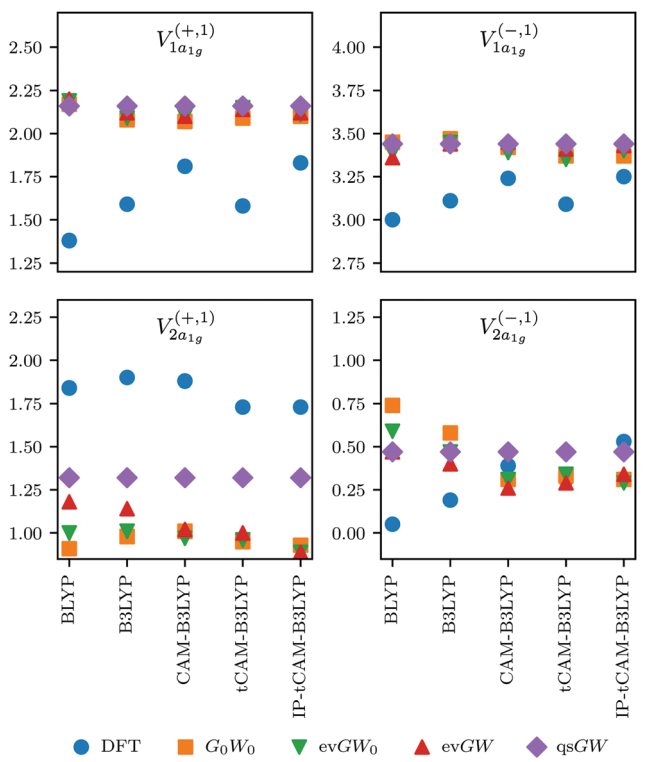

Fig. 8 Linear vibronic coupling constants of the a_{1g} normal modes for the benzene cation and anion, $V_{a_{1g}}^{(+,1)}$ and $V_{a_{1g}}^{(-,1)}$ (10^{-4} a.u.), calculated as the orbital vibronic coupling constants of the $\psi_{e_{1g}(\varepsilon)}$ and $\psi_{e_{2u}(\varepsilon)}$ orbitals of neutral benzene. The sign of $V_{a_{1g}}$ is omitted here, and the full set of orbital vibronic coupling constants is given in the ESI.†

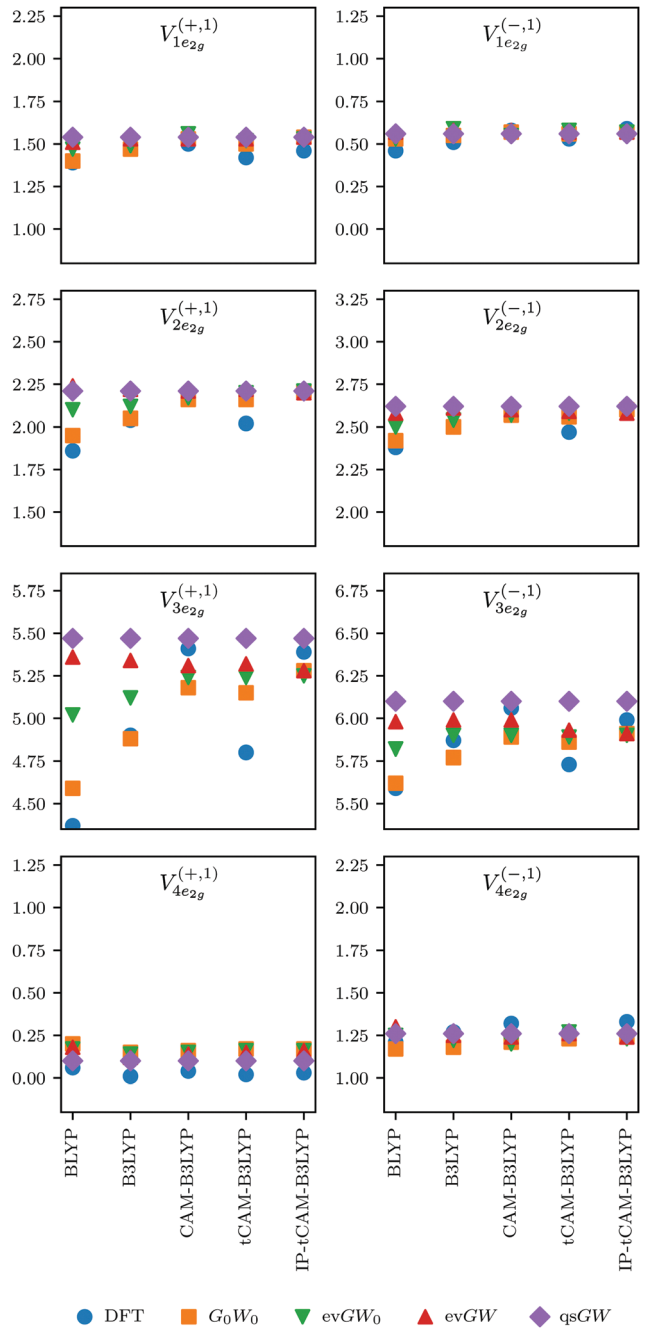

Fig. 9 Linear vibronic coupling constants of the e_{2g} normal modes for the benzene cation and anion, $V^{(+,1)}_{e_{2g}}$ and $V^{(-,1)}_{e_{2g}}$ (10^{-4} a.u.), calculated as the orbital vibronic coupling constants of the $\psi_{e_{1g}(\varepsilon)}$ and $\psi_{e_{2u}(\varepsilon)}$ orbitals of neutral benzene. The sign of $V_{e_{2g}}$ is omitted here, and the full set of orbital vibronic coupling constants is given in the ESI.†

We find that the DFT values of V_i agree well with the corresponding *GW* results for the e_{2g} normal modes. However, there is a notable difference between the *GW* and DFT results for the a_{1g} normal modes, especially in the cation. This difference in the a_{1g} results of the cation is not limited to the IP-tCAM-B3LYP functional, and can be seen in the other four functionals as well. Thus, the problem appears to be inherent to DFT itself.

A possible explanation could be the orbital relaxation effects, which are accounted for in the *GW* quasiparticle approach, but not in DFT. The frontier orbitals of neutral benzene were used to calculate V_i within DFT. In this treatment, orbital relaxation effects are ignored only in the frontier orbitals for the e_{2g} normal modes, but is ignored in all the occupied orbitals for the a_{1g} normal modes (Section 2.1). Hence, the error arising from the neglect of orbital relaxation will be smaller for the e_{2g} normal modes compared to the a_{1g} normal modes, and is a possible explanation for the difference between the DFT and *GW* results for the a_{1g} normal modes. The effect of neglecting orbital relaxation should be more significant for the energies of the occupied orbitals than the virtual orbitals, and explains the larger difference observed in the cation.

The vibrational component of vibronic coupling is then taken into account in the dimensionless vibronic coupling constants $D_i^{(+,1)}$ and $D_i^{(-,1)}$ (Fig. 10 and 11), and indicates the strength of the vibronic coupling in a normal mode. For example, the small values of D_i (<0.1) for the two C–H bond stretching modes ($2a_{1g}$ and $4e_{2g}$) imply that the vibronic coupling in these two modes is very weak.

In theory, differences between the vibrational frequencies calculated with the five DFT functionals would affect the results for $D_i^{(+,1)}$ and $D_i^{(-,1)}$. However, as the vibrational frequencies computed within the various functionals are largely similar to each other, their effect on the calculation of $D_i^{(+,1)}$ and $D_i^{(-,1)}$ becomes minimal. As a result, the trends in the results of D_i follow V_i closely, and have already been discussed earlier. Hence, we find that the electronic structure calculation is the key factor in the computational treatment of vibronic coupling, at least in the case of benzene.

The accuracy of the various *GW* methods remains to be examined. Towards this end, we first compare results from the literature to establish a suitable benchmark for our results. Literature values for $D_i^{(+,1)}$ and $D_i^{(-,1)}$ are given in Table 2.

We start with the benzene radical cation. Computationally, there is some uncertainty in the literature results from correlated wave function methods. There are two sets of CASSCF values for $D_i^{(+,1)}$ which differ from each other quite significantly. We suggest that this is because the computed values of $D_i^{(+,1)}$ in the study by Tokunaga *et al.* are scaled such that the total JT stabilisation energy (see eqn (43) below) calculated using the model vibronic Hamiltonian matches the difference between the energies of the radical at the D_{2h} and D_{6h} geometries.[83] This introduces a further dependence of their $D_i^{(+,1)}$ results on the quality of the computed geometries and vibrational frequencies, which were obtained within the relatively crude HF method. As for the difference between the CASSCF results of Applegate *et al.* and the EOMIP-CCSD values, both CASSCF and EOMIP-CCSD are capable of treating multi-reference effects, but CASSCF does not account for dynamic electron correlation.[15,114] Thus, the EOMIP-CCSD values should probably be more reliable as compared to CASSCF values. Lastly, the agreement between DFT and OVGF (outer valence Green's function) results from the literature to the EOMIP-

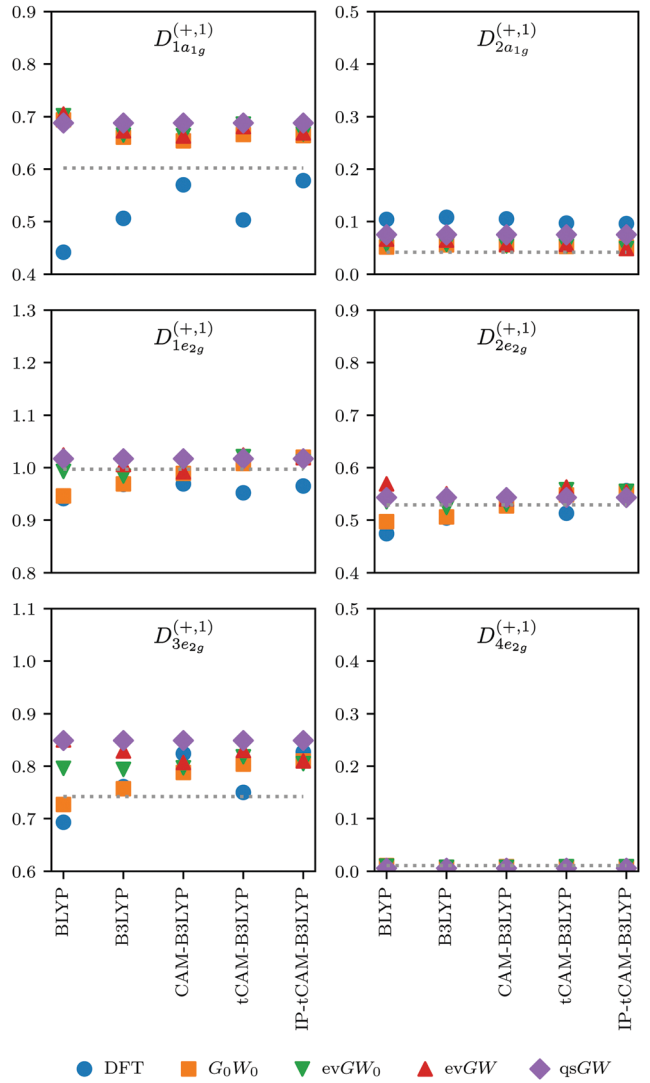

Fig. 10 DFT and *GW* dimensionless linear vibronic coupling constants of the benzene cation, $D_i^{(+,1)} = V_i^{(+,1)} \Big/ \sqrt{\hbar\omega_i^3}$, where ω_i is the vibrational frequency of the normal mode i within the respective DFT functional. The B3LYP vibrational frequencies were used in the case of qs*GW*. The horizontal grey dotted lines refer to the corresponding EOMIP-CCSD values of $D_i^{(+,1)}$.

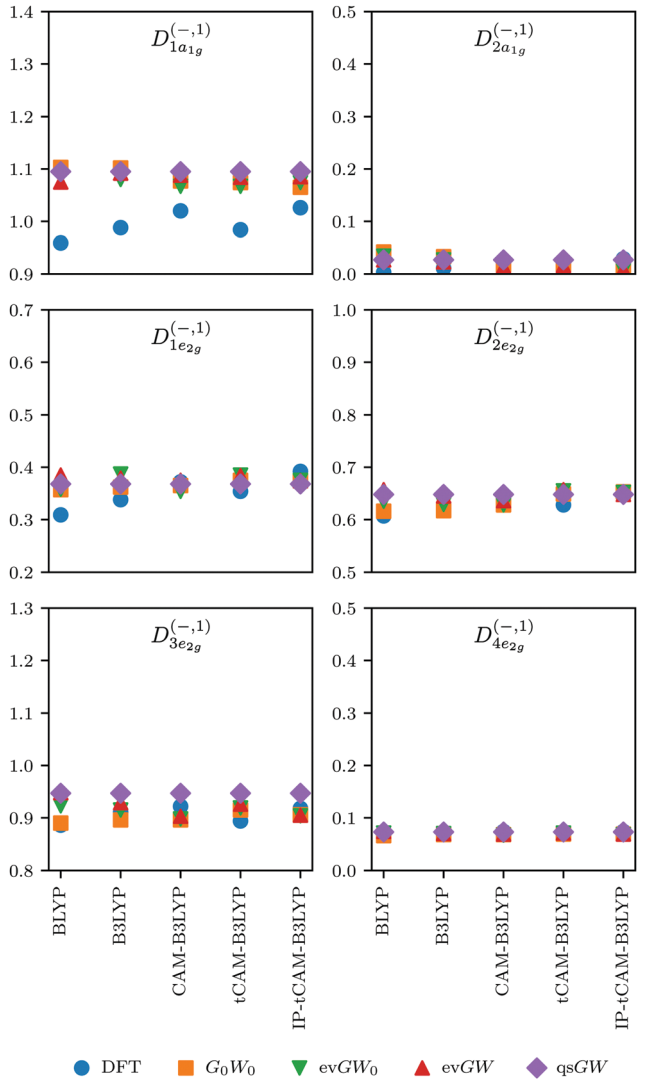

Fig. 11 DFT and *GW* dimensionless linear vibronic coupling constants of the benzene anion, $D_i^{(-,1)} = V_i^{(+,1)} \Big/ \sqrt{\hbar\omega_i^3}$, where ω_i is the vibrational frequency of the normal mode i within the respective DFT functional. The B3LYP vibrational frequencies were used in the case of qs*GW*.

CCSD values varies depending on the normal mode, but is generally quite good.

Experimentally, the values for $D^{(+,1)}_{1e_{2g}}$ and $D^{(+,1)}_{2e_{2g}}$ agree well with the EOMIP-CCSD values, but the values for $D^{(+,1)}_{3e_{2g}}$ are slightly lower in comparison. This could be because the experimental spectra are complicated by effects such as Fermi mixing at wavenumbers >1500 cm^{-1},[62,65] which is where the frequency of the $3e_{2g}$ normal mode falls into. This makes the assignment and interpretation of the experimental peaks within this range more challenging, and is a possible reason for the discrepancy between the experimental and computational results for $D^{(+,1)}_{3e_{2g}}$. Considering the above, we will use EOMIP-CCSD values as the benchmark for our benzene cation results.

We find a good agreement between our self-consistent *GW* (evGW_0, ev*GW*, and qs*GW*) results for $D_i^{(+,1)}$ and EOMIP-CCSD values (Fig. 10). The largest discrepancies in the $1a_{1g}$ and $3e_{2g}$ normal modes are small, about 0.1 only. Within the cheaper methods, the performance of G_0W_0 with long-range corrected functionals is comparable to approximate self-consistent *GW*. For DFT, CAM-B3LYP and IP-tCAM-B3LYP agree well with the self-consistent *GW* values for the e_{2g} normal modes, but not for the a_{1g} normal modes. The good agreement between the EOMIP-CCSD values of $V^{(+,1)}_{1a_{1g}}$ with the CAM-B3LYP and IP-tCAM-B3LYP results is probably due to error cancellation.

The improvement in the results using an IP-tuned functional is relatively weaker, compared to IP and EA. This could be because the IP-tuning procedure was carried out at a fixed set of nuclear coordinates, but the calculation of V_i, and hence D_i,

Table 2 Literature values of the dimensionless linear vibronic coupling constant $D_i = V_i \Big/ \sqrt{\hbar\omega_i^3}$ for the a_{1g} and e_{2g} normal modes of the benzene radical cation and anion. The computational method used for the vibrational frequencies is given in parentheses, if it differs from the method used in the electronic structure calculations

Cation	$D^{(+,1)}_{1a_{1g}}$	$D^{(+,1)}_{2a_{1g}}$	$D^{(+,1)}_{1e_{2g}}$	$D^{(+,1)}_{2e_{2g}}$	$D^{(+,1)}_{3e_{2g}}$	$D^{(+,1)}_{4e_{2g}}$
CASSCF/6-31G* (scaled HF)[65]			0.917	0.490	0.678	
CASSCF/6-31G(d,p) (HF)[83]			1.150	0.560	0.520	0.060
EOMIP-CCSD/TZ2P (CCSD)[60]	0.602	0.042	0.997	0.529	0.742	0.011
OVGF/DZP (MP2)[60]	0.706	0.066	0.983	0.510	0.800	0.008
PBE[86]			0.97	0.46	0.80	
B3LYP/6-31G*[85]	0.561		0.947	0.490	0.756	0.083
B3LYP/6-311G(2p,d)[63]			0.983	0.445	0.778	
Expt.[65]			1.010	0.490	0.600	
Expt.[62]			1.020	0.490	0.616	

Anion	$D^{(-,1)}_{1a_{1g}}$	$D^{(-,1)}_{2a_{1g}}$	$D^{(-,1)}_{1e_{2g}}$	$D^{(-,1)}_{2e_{2g}}$	$D^{(-,1)}_{3e_{2g}}$	$D^{(-,1)}_{4e_{2g}}$
CASSCF/6-31G(d,p) (HF)[83]			1.43	0.28	0.52	0.21
PBE[86]			0.16		1.06	
B3LYP/6-31G*[84]	0.953		0.408	0.613	0.969	0.063

requires a distortion of the molecular geometry. The value of the IP-tuned range-separation parameter obtained at the original, undistorted geometry would no longer be valid for the distorted molecule, and affects the calculation of the electronic states in turn. It may be possible to resolve this by carrying out the IP-tuning procedure for each distorted molecular geometry individually, but it would not be practical to do so. As such, the benefits of the IP-tuning procedure may become limited when the chemical property under study involves a change in nuclear coordinates.

After discussing the benzene cation, we consider the benzene anion. There are far fewer studies on the JT effect in the benzene radical anion. The only available set of results for $D_i^{(-,1)}$ obtained using correlated wave function methods is the CASSCF values by Tokunaga *et al.*[83] Based on their results for the benzene radical cation, the scaling of $D_i^{(-,1)}$ with respect to the energy of the radical ion at the D_{2h} and D_{6h} geometries is probably not very dependable.

Thus, because of the lack of an accurate benchmark, we will not attempt to conclusively determine the accuracy of *GW* towards vibronic coupling in the benzene radical anion, and restrict the analysis of the benzene anion to a comparison within our own results. Compared to the benzene cation, there is a better agreement in the values of $D_i^{(-,1)}$ across the various *GW* methods and DFT. As mentioned above, the largest difference between DFT and *GW* is observed in the $1a_{1g}$ normal mode. Considering the agreement within our computational results for the benzene anion, as well as the general performance of *GW* with respect to the benzene cation, we suggest that our *GW* results for the benzene anion should also be reasonably accurate.

After examining the quality of our computational results, we discuss the JT distortion in the benzene radical cation and anion. We will not consider the C–H bond stretching modes because they do not contribute significantly to the JT effect in the benzene radical ions.

The JT stabilisation energy E_i^{JT} for normal mode i is calculated as

$$E_i^{JT} = \frac{\hbar\omega_i}{2} D_i^2 \tag{43}$$

If the value of D_i for a normal mode i is greater than 1, the JT stabilisation energy for i is larger than its zero-point vibrational energy, and the molecule would undergo a static JT distortion along i. This just about holds for the first e_{1g} normal mode for the benzene cation, and implies that the cation will be distorted to a D_{2h} geometry along this mode.

For the benzene anion, $D_i^{(-,1)}$ is greater than 1 only for the $1a_{1g}$ mode in the benzene anion, which is the totally symmetric C–C bond stretching mode. Interestingly, the $1a_{1g}$ normal mode is not usually classified as a JT active mode because it does not lower the D_{6h} point group symmetry of the system. Despite this, we can use this result to predict that the C–C bonds are lengthened in the benzene radical anion compared to neutral benzene, which agrees with the literature.[79]

For the other normal modes in the benzene cation and anion, D_i is less than 1, and the system undergoes pseudorotation following the minimum energy path in the 'Mexican hat' potential (Fig. 12). The calculation of the pseudorotation barrier would involve extending the linear vibronic coupling model used in the present study to include quadratic vibronic coupling terms. A brief examination of the quadratic vibronic coupling constants of the e_{2g} and a_{1g} normal modes confirms that the quadratic JT effect for these modes is weak (ESI†). Hence, there is effectively no pseudorotation barrier in the benzene cation or anion, which is in agreement with the literature.[63,65,66,68,70,72,75,77,79,81]

In sum, we investigated vibronic coupling using different levels of the *GW* approximation. In the case of benzene, we find that the main determining factor behind the computation of vibronic coupling constants is the electronic structure calculations. Thus, *GW* methods perform well because of their accuracy with respect to the molecular electronic properties.

In particular, the approximate self-consistent *GW* methods consistently returned the most accurate vibronic coupling constants. Although the starting point dependence of G_0W_0 is reduced compared to the IP and EA, the choice of the original DFT functional remains significant, with long-range corrected functionals found to give the best results with G_0W_0. Based on the results of the present study and our earlier work on the cyclopentadienyl radical,[47] we suggest that range-separated functionals are a good starting point for G_0W_0 calculations. Also, the effectiveness of the IP-tuning procedure appears to be reduced for the computation of vibronic coupling constants, which is ascribed to the computational protocol used in the calculation.

Finally, we note that the vibrational frequencies used for computing D_i were still obtained within DFT, and not *GW*. This was because the numerical calculation of the vibrational frequencies as the second derivative of the Galitski–Migdal total energies was not found to improve upon DFT. However, there are some recent studies on the total energies and molecular PES within *GW* which may prove otherwise. Bruneval

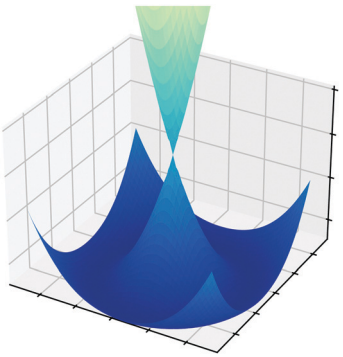

Fig. 12 A 'Mexican hat' plot of the potential energy surface of the benzene radical cation. The benzene cation undergoes pseudorotation along the minimum energy path.

has defined a '*GW* density matrix' to calculate the total energy within *GW*,[115,116] while Loos and co-workers have examined the ground state PES of diatomic molecules using the Bethe–Salpeter equation within the adiabatic-connection fluctuation-dissipation theorem.[117,118] These studies may offer the possibility of improved vibrational frequencies, and hence improved vibronic coupling constants that are obtained completely within *GW*.

Other than this, we did not consider higher order vibronic coupling terms, such as intermode coupling or the quadratic coupling in normal modes that are not of e_{2g} or a_{1g} symmetry, in this work. A study on the benzene anion by Bazante *et al.* found a C_2 non-planar minimum energy geometry for the benzene radical anion,[79] which is not possible within the linear vibronic coupling model of the present study. The inclusion of higher order vibronic coupling terms in the vibronic Hamiltonian, *e.g.*, the coupling between e_{2u} normal modes, is necessary to model the out-of-plane bending.

Also, we only looked at the JT coupling in the ground electronic state of the benzene radical cation and anion. Thus, another possible extension of the present work would be to include pseudo-JT coupling in the lower electronic states of the radical ions. This has been investigated in some earlier studies,[56–64] and would test the applicability of *GW* beyond the frontier orbitals of benzene. We are currently carrying out some exploratory work in this direction.

5 Conclusion

The main goal of this paper was to investigate the calculation of vibronic coupling constants using a hierarchy of *GW*-based methods. We approached this problem by considering the individual components of vibronic coupling, and analysed the performance of *GW* towards the electronic and vibrational properties of benzene.

The electronic properties of benzene were examined by calculating its IP and EA, and we confirmed that approximate self-consistent *GW* methods provide the best agreement with CCSD(T) values from the literature. With the exception of the IP-tuned CAM-B3LYP functional, DFT was found to perform poorly in this regard, but the G_0W_0 correction resulted in a significant improvement throughout.

Next, the vibrational frequencies of the a_{1g} and e_{2g} normal modes of benzene were calculated numerically as the second derivatives of the SCF and Galitski–Migdal total energies for DFT and *GW*, respectively. In this case, the *GW* results were slightly poorer than their DFT counterparts. In addition, the differences across the DFT vibrational frequencies calculated using the different exchange–correlation functionals were found to be quite small as well. As a result, we observed that the computation of vibronic coupling constants is mainly influenced by the electronic state calculations.

Finally, using the B3LYP normal modes of neutral benzene, the vibronic coupling constants of the benzene radical cation and anion were obtained numerically as the gradients of the frontier orbitals of neutral benzene for DFT, while the gradients of the corresponding quasiparticle energies were used in the case of *GW*. On the whole, we find that the starting point dependency of the computed vibronic coupling constants becomes negligible with approximate self-consistent *GW* methods, and these methods provide results that agree well with EOMIP-CCSD values from the literature. G_0W_0 with long-range corrected functionals also yielded results that are comparable to those of self-consistent *GW*, while those of DFT are slightly poorer.

In particular, the DFT treatment of the vibronic coupling constants for the a_{1g} normal modes assumes that all occupied orbitals are frozen, which is why the DFT results for these modes are poorer than those for the e_{2g} normal modes, in which it only assumes the frontier orbitals to be frozen. The calculation of vibronic coupling constants using the quasiparticle energies within *GW* does not require any such approximation, and agrees better with the high level wave function methods on the whole.

Conflicts of interest

There are no conflicts to declare.

Acknowledgements

Scientific grants R-143-000-A80-114 and R-143-000-A65-133 from the Ministry of Education, Singapore are gratefully acknowledged. Computational resources from the National Supercomputing Centre (ASPIRE-1, grant 11001278) and the High Performance Computing Services at the National University of Singapore (NUS) Computer Centre were used for this study.

References

1 H. Mustroph, *ChemPhysChem*, 2016, **17**, 2616–2629.
2 F. Jensen, *Introduction to Computational Chemistry*, John Wiley & Sons, Inc., 3rd edn, 2016, p. 660.

3 C. J. Cramer, *Essentials of Computational Chemistry: Theories and Models*, John Wiley & Sons, Inc., 2nd edn, 2004, p. 618.
4 G. J. Rocklin, T. M. Chidyausiku, I. Goreshnik, A. Ford, S. Houliston, A. Lemak, L. Carter, R. Ravichandran, V. K. Mulligan, A. Chevalier, C. H. Arrowsmith and D. Baker, *Science*, 2017, **357**, 168–175.
5 Q. Shao, J. Shi and W. Zhu, *J. Chem. Theory Comput.*, 2017, **13**, 1229–1243.
6 I. B. Bersuker and V. Z. Polinger, *Vibronic Interactions in Molecules and Crystals*, Springer-Verlag, Berlin, Heidelberg, 1989.
7 G. Fischer, *Vibronic coupling: The Interaction Between the Electronic and Nuclear Motions*, Academic Press, 1984, vol. 9.
8 H. A. Jahn and E. Teller, *Proc. R. Soc. London, Ser. A*, 1937, **161**, 220–235.
9 J. D. Watts, J. Gauss and R. J. Bartlett, *J. Chem. Phys.*, 1993, **98**, 8718–8733.
10 K. Raghavachari, G. W. Trucks, J. A. Pople and M. Head-Gordon, *Chem. Phys. Lett.*, 1989, **157**, 479–483.
11 K. Andersson, P.-Å. Malmqvist and B. O. Roos, *J. Chem. Phys.*, 1992, **96**, 1218–1226.
12 K. Andersson, P.-Å. Malmqvist, B. O. Roos, A. J. Sadlej and K. Wolinski, *J. Phys. Chem.*, 1990, **94**, 5483–5488.
13 R. J. Bartlett and M. Musiał, *Rev. Mod. Phys.*, 2007, **79**, 291–352.
14 R. J. Bartlett, in *Coupled-cluster theory in quantum chemistry*, ed. C. E. Dykstra, G. Frenking, K. S. Kim and G. E. Scuseria, How and why coupled-cluster theory became the preeminent method in an *ab initio* quantum chemistry, Elsevier, Amsterdam, 2005, pp. 1191–1221.
15 B. O. Roos, R. Lindh, P. Å. Malmqvist, V. Veryazov and P.-O. Widmark, *Multiconfigurational Quantum Chemistry*, John Wiley & Sons, Inc., 2016.
16 P. Pulay, *Int. J. Quantum Chem.*, 2011, **111**, 3273–3279.
17 P. Verma and D. G. Truhlar, *Trends Chem.*, 2020, **2**, 302–318.
18 H. S. Yu, S. L. Li and D. G. Truhlar, *J. Chem. Phys.*, 2016, **145**, 130901.
19 A. J. Cohen, P. Mori-Sánchez and W. Yang, *Chem. Rev.*, 2011, **112**, 289–320.
20 D. Hait and M. Head-Gordon, *J. Chem. Theory Comput.*, 2018, **14**, 1969–1981.
21 L. Goerigk, A. Hansen, C. Bauer, S. Ehrlich, A. Najibi and S. Grimme, *Phys. Chem. Chem. Phys.*, 2017, **19**, 32184–32215.
22 N. Mardirossian and M. Head-Gordon, *Mol. Phys.*, 2017, **115**, 2315–2372.
23 A. M. Teale, O. B. Lutnæs, T. Helgaker, D. J. Tozer and J. Gauss, *J. Chem. Phys.*, 2013, **138**, 024111.
24 M. G. Medvedev, I. S. Bushmarinov, J. Sun, J. P. Perdew and K. A. Lyssenko, *Science*, 2017, **355**, 49–52.
25 A. Kreppel, D. Graf, H. Laqua and C. Ochsenfeld, *J. Chem. Theory Comput.*, 2020, **16**, 2985–2994.
26 A. Ottochian, C. Morgillo, I. Ciofini, M. J. Frisch, G. Scalmani and C. Adamo, *J. Comput. Chem.*, 2020, **41**, 1242–1251.
27 D. Golze, M. Dvorak and P. Rinke, *Front. Chem.*, 2019, **7**, 377.
28 L. Reining, *Wiley Interdiscip. Rev.: Comput. Mol. Sci.*, 2017, **8**, e1344.
29 R. M. Martin, L. Reining and D. M. Ceperley, *Interacting Electrons: Theory and Computational Approaches*, Cambridge University Press, 2016.
30 L. Hedin, *Phys. Rev.*, 1965, **139**, A796–A823.
31 M. J. van Setten, F. Caruso, S. Sharifzadeh, X. Ren, M. Scheffler, F. Liu, J. Lischner, L. Lin, J. R. Deslippe, S. G. Louie, C. Yang, F. Weigend, J. B. Neaton, F. Evers and P. Rinke, *J. Chem. Theory Comput.*, 2015, **11**, 5665–5687.
32 M. J. van Setten, F. Weigend and F. Evers, *J. Chem. Theory Comput.*, 2012, **9**, 232–246.
33 L. Gallandi, N. Marom, P. Rinke and T. Körzdörfer, *J. Chem. Theory Comput.*, 2016, **12**, 605–614.
34 F. Caruso, M. Dauth, M. J. van Setten and P. Rinke, *J. Chem. Theory Comput.*, 2016, **12**, 5076–5087.
35 X. Blase, C. Attaccalite and V. Olevano, *Phys. Rev. B: Condens. Matter Mater. Phys.*, 2011, **83**, 115103.
36 C. Faber, C. Attaccalite, V. Olevano, E. Runge and X. Blase, *Phys. Rev. B: Condens. Matter Mater. Phys.*, 2011, **83**, 115123.
37 F. Bruneval and M. A. L. Marques, *J. Chem. Theory Comput.*, 2013, **9**, 324–329.
38 F. Kaplan, M. E. Harding, C. Seiler, F. Weigend, F. Evers and M. J. van Setten, *J. Chem. Theory Comput.*, 2016, **12**, 2528–2541.
39 M. Shishkin and G. Kresse, *Phys. Rev. B: Condens. Matter Mater. Phys.*, 2007, **75**, 235102.
40 A. Stan, N. E. Dahlen and R. van Leeuwen, *J. Chem. Phys.*, 2009, **130**, 114105.
41 M. van Schilfgaarde, T. Kotani and S. V. Faleev, *Phys. Rev. Lett.*, 2006, **96**, 226402.
42 T. Kotani, M. van Schilfgaarde and S. V. Faleev, *Phys. Rev. B: Condens. Matter Mater. Phys.*, 2007, **76**, 165106.
43 J. W. Knight, X. Wang, L. Gallandi, O. Dolgounitcheva, X. Ren, J. V. Ortiz, P. Rinke, T. Körzdörfer and N. Marom, *J. Chem. Theory Comput.*, 2016, **12**, 615–626.
44 T. Rangel, S. M. Hamed, F. Bruneval and J. B. Neaton, *J. Chem. Theory Comput.*, 2016, **12**, 2834–2842.
45 L. Gallandi and T. Körzdörfer, *J. Chem. Theory Comput.*, 2015, **11**, 5391–5400.
46 N. Marom, F. Caruso, X. Ren, O. T. Hofmann, T. Körzdörfer, J. R. Chelikowsky, A. Rubio, M. Scheffler and P. Rinke, *Phys. Rev. B: Condens. Matter Mater. Phys.*, 2012, **86**, 245127.
47 Z. C. Wong and L. Ungur, *J. Chem. Phys.*, 2020, **153**, 064303.
48 Z. Li, G. Antonius, M. Wu, F. H. da Jornada and S. G. Louie, *Phys. Rev. Lett.*, 2019, **122**, 186402.
49 P. Koval, M. P. Ljungberg, M. Müller and D. Sánchez-Portal, *J. Chem. Theory Comput.*, 2019, **15**, 4564–4580.
50 F. Karsai, M. Engel, E. Flage-Larsen and G. Kresse, *New J. Phys.*, 2018, **20**, 123008.
51 C. Faber, P. Boulanger, C. Attaccalite, E. Cannuccia, I. Duchemin, T. Deutsch and X. Blase, *Phys. Rev. B: Condens. Matter Mater. Phys.*, 2015, **91**, 155109.

52 Z. P. Yin, A. Kutepov and G. Kotliar, *Phys. Rev. X*, 2013, **3**, 021011.
53 C. Faber, I. Duchemin, T. Deutsch, C. Attaccalite, V. Olevano and X. Blase, *J. Mater. Sci.*, 2012, **47**, 7472–7481.
54 C. Faber, J. L. Janssen, M. Côté, E. Runge and X. Blase, *Phys. Rev. B: Condens. Matter Mater. Phys.*, 2011, **84**, 155104.
55 M. Lazzeri, C. Attaccalite, L. Wirtz and F. Mauri, *Phys. Rev. B: Condens. Matter Mater. Phys.*, 2008, **78**, 081406.
56 S. Scheit, S. Goswami, H.-D. Meyer and H. Köppel, *Comput. Theor. Chem.*, 2019, **1150**, 71–84.
57 M. C. E. Galbraith, S. Scheit, N. V. Golubev, G. Reitsma, N. Zhavoronkov, V. Despré, F. Lépine, A. I. Kuleff, M. J. J. Vrakking, O. Kornilov, H. Köppel and J. Mikosch, *Nat. Commun.*, 2017, **8**, 1018.
58 I. Bâldea and H. Köppel, *J. Chem. Phys.*, 2006, **124**, 064101.
59 H. Köppel, I. Bâldea and P. G. Szalay, *Advances in Quantum Chemistry*, Elsevier, 2003, pp. 199–217.
60 M. Döscher, H. Köppel and P. G. Szalay, *J. Chem. Phys.*, 2002, **117**, 2645–2656.
61 H. Köppel, M. Döscher, I. Bâldea, H.-D. Meyer and P. G. Szalay, *J. Chem. Phys.*, 2002, **117**, 2657–2671.
62 A. B. Burrill, Y. K. Chung, H. A. Mann and P. M. Johnson, *J. Chem. Phys.*, 2004, **120**, 8587–8599.
63 P. M. Johnson, *J. Chem. Phys.*, 2002, **117**, 9991–10000.
64 P. M. Johnson, *J. Chem. Phys.*, 2002, **117**, 10001–10007.
65 B. E. Applegate and T. A. Miller, *J. Chem. Phys.*, 2002, **117**, 10654–10674.
66 M. L. Vidal, M. Epshtein, V. Scutelnic, Z. Yang, T. Xue, S. R. Leone, A. I. Krylov and S. Coriani, *J. Phys. Chem. A*, 2020, **124**, 9532–9541.
67 M. Epshtein, V. Scutelnic, Z. Yang, T. Xue, M. L. Vidal, A. I. Krylov, S. Coriani and S. R. Leone, *J. Phys. Chem. A*, 2020, **124**, 9524–9531.
68 H. Tachikawa, *J. Phys. Chem. A*, 2018, **122**, 4121–4129.
69 I. Bâldea, *RSC Adv.*, 2016, **6**, 93715–93721.
70 M. Gruden-Pavlović, P. García-Fernández, L. Andjelković, C. Daul and M. Zlatar, *J. Phys. Chem. A*, 2011, **115**, 10801–10813.
71 C. H. Kwon, H. L. Kim and M. S. Kim, *J. Chem. Phys.*, 2003, **119**, 215–223.
72 M. S. Deleuze, L. Claes, E. S. Kryachko and J.-P. François, *J. Chem. Phys.*, 2003, **119**, 3106–3119.
73 J. M. Bakker, R. G. Satink, G. von Helden and G. Meijer, *Phys. Chem. Chem. Phys.*, 2002, **4**, 24–33.
74 A. Fujii, E. Fujimaki, T. Ebata and N. Mikami, *J. Chem. Phys.*, 2000, **112**, 6275–6284.
75 K. Müller-Dethlefs and J. B. Peel, *J. Chem. Phys.*, 1999, **111**, 10550–10554.
76 J. G. Goode, J. D. Hofstein and P. M. Johnson, *J. Chem. Phys.*, 1997, **107**, 1703–1716.
77 R. Lindner, K. Müller-Dethlefs, E. Wedum, K. Haber and E. R. Grant, *Science*, 1996, **271**, 1698–1702.
78 K. Brezina, P. Jungwirth and O. Marsalek, *J. Phys. Chem. Lett.*, 2020, **11**, 6032–6038.
79 A. P. Bazante, E. R. Davidson and R. J. Bartlett, *J. Chem. Phys.*, 2015, **142**, 204304.
80 B. Hajgató, M. S. Deleuze, D. J. Tozer and F. D. Proft, *J. Chem. Phys.*, 2008, **129**, 084308.
81 I. V. Beregovaya and L. N. Shchegoleva, *Int. J. Quantum Chem.*, 2002, **88**, 481–488.
82 J. C. Rienstra-Kiracofe, C. J. Barden, S. T. Brown and H. F. Schaefer, *J. Phys. Chem. A*, 2001, **105**, 524–528.
83 K. Tokunaga, T. Sato and K. Tanaka, *J. Chem. Phys.*, 2006, **124**, 154303.
84 T. Kato and K. Hirao, *Advances in Quantum Chemistry*, Elsevier, 2003, pp. 257–271.
85 T. Kato and T. Yamabe, *J. Chem. Phys.*, 2001, **115**, 8592–8602.
86 V. Perebeinos, P. B. Allen and M. Pederson, *Phys. Rev. A: At., Mol., Opt. Phys.*, 2005, **72**, 012501.
87 T. Sato, K. Tokunaga and K. Tanaka, *J. Chem. Phys.*, 2006, **124**, 024314.
88 T. Azumi and K. Matsuzaki, *Photochem. Photobiol.*, 1977, **25**, 315–326.
89 A. D. Liehr, *J. Phys. Chem.*, 1963, **67**, 389–471.
90 A. Szabo and N. S. Ostlund, *Modern Quantum Chemistry: Introduction to Advanced Electronic Structure Theory*, Dover Publications, Inc., New York, 1996.
91 I. B. Bersuker, *Chem. Rev.*, 2020, **121**, 1463–1512.
92 I. B. Bersuker, *Chem. Rev.*, 2001, **101**, 1067–1114.
93 T. Inui, Y. Tanabe and Y. Onodera, *Group Theory and Its Applications in Physics*, Springer-Verlag, Berlin, Heidelberg, 1990.
94 S. L. Altmann and P. Herzig, *Point-Group Theory Tables*, Clarendon Press, Oxford, 2nd edn, 2011.
95 I. B. Bersuker, *J. Comput. Chem.*, 1997, **18**, 260–267.
96 A. D. Becke, *J. Chem. Phys.*, 1993, **98**, 5648–5652.
97 P. J. Stephens, F. J. Devlin, C. F. Chabalowski and M. J. Frisch, *J. Phys. Chem.*, 1994, **98**, 11623–11627.
98 F. Weigend and R. Ahlrichs, *Phys. Chem. Chem. Phys.*, 2005, **7**, 3297.
99 M. J. Frisch, G. W. Trucks, H. B. Schlegel, G. E. Scuseria, M. A. Robb, J. R. Cheeseman, G. Scalmani, V. Barone, G. A. Petersson, H. Nakatsuji, X. Li, M. Caricato, A. V. Marenich, J. Bloino, B. G. Janesko, R. Gomperts, B. Mennucci, H. P. Hratchian, J. V. Ortiz, A. F. Izmaylov, J. L. Sonnenberg, D. Williams-Young, F. Ding, F. Lipparini, F. Egidi, J. Goings, B. Peng, A. Petrone, T. Henderson, D. Ranasinghe, V. G. Zakrzewski, J. Gao, N. Rega, G. Zheng, W. Liang, M. Hada, M. Ehara, K. Toyota, R. Fukuda, J. Hasegawa, M. Ishida, T. Nakajima, Y. Honda, O. Kitao, H. Nakai, T. Vreven, K. Throssell, J. A. Montgomery, Jr., J. E. Peralta, F. Ogliaro, M. J. Bearpark, J. J. Heyd, E. N. Brothers, K. N. Kudin, V. N. Staroverov, T. A. Keith, R. Kobayashi, J. Normand, K. Raghavachari, A. P. Rendell, J. C. Burant, S. S. Iyengar, J. Tomasi, M. Cossi, J. M. Millam, M. Klene, C. Adamo, R. Cammi, J. W. Ochterski, R. L. Martin, K. Morokuma, O. Farkas, J. B. Foresman and D. J. Fox, *Gaussian16 Revision A.01*, Gaussian Inc., Wallingford CT, 2016.
100 F. Bruneval, T. Rangel, S. M. Hamed, M. Shao, C. Yang and J. B. Neaton, *Comput. Phys. Commun.*, 2016, **208**, 149–161.

101 A. D. Becke, *Phys. Rev. A: At., Mol., Opt. Phys.*, 1988, **38**, 3098–3100.
102 C. Lee, W. Yang and R. G. Parr, *Phys. Rev. B: Condens. Matter Mater. Phys.*, 1988, **37**, 785–789.
103 T. Yanai, D. P. Tew and N. C. Handy, *Chem. Phys. Lett.*, 2004, **393**, 51–57.
104 K. Okuno, Y. Shigeta, R. Kishi, H. Miyasaka and M. Nakano, *J. Photochem. Photobiol., A*, 2012, **235**, 29–34.
105 J. Bois and T. Körzdörfer, *J. Chem. Theory Comput.*, 2017, **13**, 4962–4971.
106 F. Weigend, *Phys. Chem. Chem. Phys.*, 2006, **8**, 1057.
107 R. A. Mata and M. A. Suhm, *Angew. Chem., Int. Ed.*, 2017, **56**, 11011–11018.
108 F. Bruneval, I. Maliyov, C. Lapointe and M.-C. Marinica, *J. Chem. Theory Comput.*, 2020, **16**, 4399–4407.
109 M. Govoni and G. Galli, *J. Chem. Theory Comput.*, 2018, **14**, 1895–1909.
110 J. Wilhelm, M. D. Ben and J. Hutter, *J. Chem. Theory Comput.*, 2016, **12**, 3623–3635.
111 E. Maggio, P. Liu, M. J. van Setten and G. Kresse, *J. Chem. Theory Comput.*, 2017, **13**, 635–648.
112 V. M. Galitskii and A. B. Migdal, *J. Exp. Theor. Phys.*, 1958, **34**, 96–104.
113 R. D. Johnson, *NIST Computational Chemistry Comparison and Benchmark Database*, 1999, https://cccbdb.nist.gov.
114 J. F. Stanton, *J. Chem. Phys.*, 2001, **115**, 10382.
115 F. Bruneval, M. Rodriguez-Mayorga, P. Rinke and M. Dvorak, *J. Chem. Theory Comput.*, 2021, **17**, 2126–2136.
116 F. Bruneval, *J. Chem. Theory Comput.*, 2019, **15**, 4069–4078.
117 P.-F. Loos, A. Scemama, I. Duchemin, D. Jacquemin and X. ier Blase, *J. Phys. Chem. Lett.*, 2020, **11**, 3536–3545.
118 J. A. Berger, P.-F. Loos and P. Romaniello, *J. Chem. Theory Comput.*, 2020, **17**, 191–200.

